Journal of
Materials Chemistry A

Accepted Manuscript

This article can be cited before page numbers have been issued, to do this please use: R. Prasad, S. Seidner, D. B. Cordes, M. Lozinska, D. Dawson, M. Thompson, T. Düren, K. Chakarova, M. Mihaylov, K. Hadjiivanov, F. Hoffmann, A. Slawin, S. E. Ashbrook, M. Clarke and P. Wright, *J. Mater. Chem. A*, 2019, DOI: 10.1039/C8TA10610J.

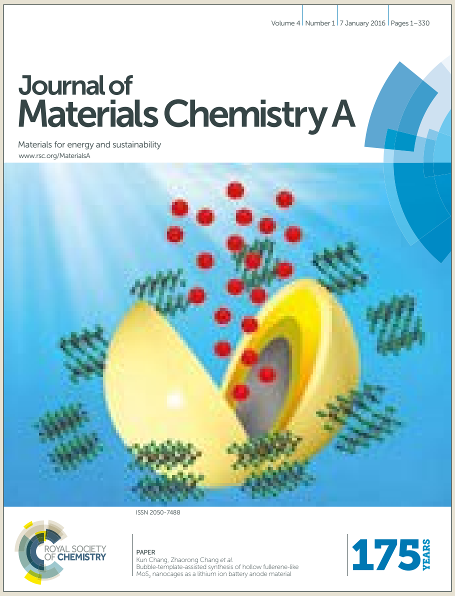

View Article Online
DOI: 10.1039/C8TA10610J

STA-27, a porous Lewis acidic scandium MOF with an unexpected topology type prepared with 2,3,5,6-tetrakis(4-carboxyphenyl)pyrazine

Ram R. R. Prasad,[a] Sarah E. Seidner,[a] David B. Cordes,[a] Magdalena M. Lozinska,[a] Daniel M. Dawson,[a] Megan J. Thompson,[b] Tina Düren,[b] Kristina K. Chakarova,[c] Mihail Y. Mihaylov,[c] Konstantin I. Hadjiivanov,[c] Frank Hoffmann,[d] Alexandra M. Z. Slawin,[a] Sharon. E. Ashbrook,[a] Matthew L. Clarke [a] and Paul A. Wright[a*]

[a] EaStCHEM School of Chemistry, University of St Andrews, Purdie Building, North Haugh, St Andrews, KY16 9ST, UK.
[b] Centre for Advanced Separations Engineering, Department of Chemical Engineering, University of Bath, Bath, BA2 7AY, UK.
[c] Institute of General and Inorganic Chemistry, Bulgarian Academy of Sciences, Sofia 1113, Bulgaria.
[d] Institute of Inorganic and Applied Chemistry, Department of Chemistry, University of Hamburg, Martin-Luther-King-Platz 6, 20146 Hamburg, Germany.

*E-mail : paw2@st-andrews.ac.uk

Abstract: A porous scandium MOF denoted STA-27 (St Andrews Porous Material-27) has been synthesised solvothermally using the 2,3,5,6-tetrakis(4-carboxyphenyl)pyrazine anion ($TCPP^{4-}$) as the tetratopic carboxylate linker. STA-27 possesses a unique scandium-based 1D rod secondary building unit (SBU) comprising corner-sharing scandium Sc_2O_{11} dimers connected via carboxylate groups from the linker. After activation under mild conditions STA-27 is an active Lewis acidic catalyst, while heating at elevated temperatures results in rupturing of the Sc-O-Sc linkages and a phase transition to a different topological type. Under similar synthesis conditions the smaller Al^{3+} and Ga^{3+} cations give isostructural MOFs with a different, previously reported, topology type based on chains of corner-sharing $MO_4(OH)_2$ octahedra: the Al-form possesses attractive properties for CO_2 adsorption.

Introduction

Reticular chemistry, the underlying principle of which is the designed assembly of metal cation-based nodes and polytopic organic linkers, has been used to great effect in the preparation of numerous families of porous metal organic frameworks (MOFs).[1-5] Among these, the carboxylates MIL-53,[6] -88,[7] -100,[8] -101,[9] *soc*-MOF[10] and MFM-300[11] of the trivalent metal cations Al^{3+}, Cr^{3+}, Fe^{3+} and Ga^{3+} are some of the most intensely studied MOFs for potential applications in adsorption, separation, drug delivery and catalysis. In these

View Article Online
DOI: 10.1039/C8TA10610J

materials, the metal cation-based inorganic nodes take the form of corner-sharing chains or trimers of MO_6 octahedra, as shown in Figure 1.

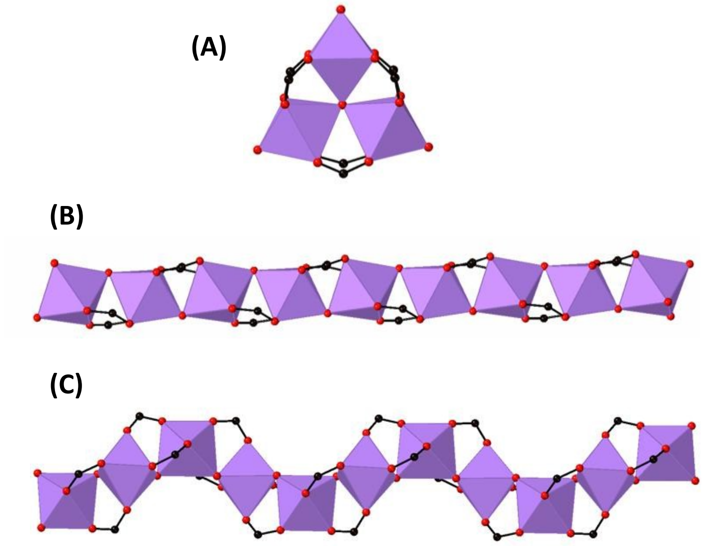

Figure 1. Observed SBUs in M^{3+}-based MOFs: (A) trimer-based SBUs of MIL-88, -100, -101 and *soc*MOF, (B) 1D rod SBU of MIL-53 family and (C) 1D rod SBU of MFM-300.

It is possible to prepare Sc^{3+} analogues of these carboxylate MOFs, where the slightly larger Sc^{3+} cations (ionic radius 0.745 Å vs 0.675 Å (Al^{3+})) adopt octahedral coordination in the chain or trimer building units, modifying the breathing behaviour of MIL-53 and imparting highly effective Lewis acidic catalytic sites to MIL-100, for example.[12] Additionally, it is possible to prepare porous MOFs with Sc^{3+} within the metal nodes that are structurally different from those prepared with the other cations, due to its larger radius.[13-15] These include Sc_2BDC_3, a highly stable MOF, not been prepared for metals other than scandium, which displays a unique set of properties for the adsorption of molecules such as CO_2 and light alkanes.[14] Despite the attractive properties for adsorption and catalysis reported above, the area of Sc MOFs remains relatively little studied, and so the investigation of tetracarboxylate Sc-MOFs was deemed timely, as only three had been reported, NOTT-401[16a] and the scandium analogues of In-*soc*-MOF[12a,c] and MFM-300.[16b] 2,3,5,6-Tetrakis(4-carboxyphenyl)pyrazine (H_4TCPP, Scheme 1) is readily-prepared and its use had only been reported rarely in MOF synthesis.[17] We anticipated that the resulting linker $TCPP^{4-}$ (hereafter TCPP) would give tetracarboxylate scandium MOFs with interesting adsorptive and catalytic properties.

View Article Online
DOI: 10.1039/C8TA10610J

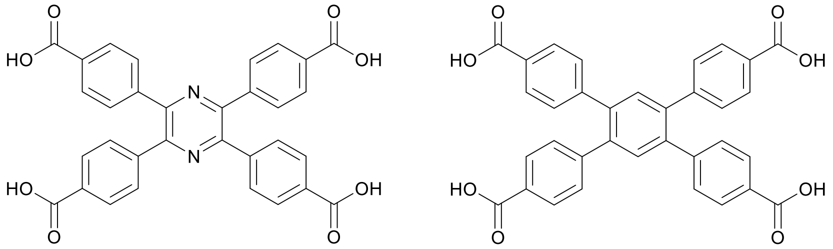

Scheme 1 Structure of the acid forms of the linkers TCPP (left) and TCPB (right).

Here we describe the results of syntheses of TCPP-based MOFs with Sc^{3+}, as well as those carried out with the trivalent metal cations Al^{3+} and Ga^{3+} for comparison. The latter two cations give structural analogues of the reported Al-MOF, $[Al_2(OH)_2(TCPB)]$[18] prepared from the similar acid 2,3,5,6-tetrakis(4-carboxyphenyl)benzene (H_4TCPB, Scheme 1), as might have been predicted by reticular chemistry. By conrast, the use of Sc^{3+} results in STA-27, a microporous 3D-connected scandium MOF with an unprecedented infinite rod building unit. We describe its adsorptive and Lewis acidic catalytic properties and report that it undergoes a structural phase transition at elevated temperature.

Experimental

Synthesis of H_4TCPP

H_4TCPP was synthesised in two steps by modifying the reported procedure.[17] The synthesis procedure and details of its characterization are given in the ESI.

Synthesis of $Al_2(OH)_2TCPP$

$Al_2(OH)_2TCPP$ was synthesised in a mixed solvent system of N, N-dimethylformamide (DMF) and nitric acid (HNO_3). 190.6 mg $Al(NO_3)_3.9H_2O$ or 216.1 mg $AlCl_3.6H_2O$ (0.895 mmol) and 41.2 mg H_4TCPP (0.074 mmol) were weighed out into a Teflon-liner (total volume ~ 30 mL) equipped with a magnetic stirrer bar. 7.5 mL of DMF followed by 7.5 mL of 3.5 M aq. HNO_3 were added to the mixture using either a syringe or measuring cylinder. The solution was stirred at room temperature until it turned pale yellow (usually 45-50 min). The stirrer bar was removed, and the Teflon-liner was placed inside a stainless-steel autoclave before heating in a pre-heated oven at 150 °C for 30 h. After cooling to room temperature at a rate of 5 °C min^{-1}, the resulting white powder was filtered and washed multiple times with DMF, followed by methanol and kept in methanol overnight before filtering and drying at 80 °C overnight. Calc. C, 47.93; H, 2.98; N, 4.55 wt%. Meas. C, 48.01; H, 2.90; N, 4.45 wt%.

Synthesis of $Ga_2(OH)_2$TCPP

$Ga_2(OH)_2$TCPP was synthesised in DMF and HNO_3 similarly to $Al_2(OH)_2$TCPP: 228.8 mg $Ga(NO_3)_3.6H_2O$ (0.628 mmol) and 41.2 mg H_4TCPP (0.074 mmol) were weighed into a Teflon-liner (total volume ~30 mL) equipped with a magnetic stirrer bar. 7.5 mL of DMF followed by the same volume of3.5 M aq. HNO_3 was added to the mixture using either a syringe or measuring cylinder. The solution was stirred at room temperature until the colour of the solution changed to pale yellow (usually 45-50 min). The stirrer bar was removed, and the Teflon-liner was placed inside a stainless-steel autoclave before heating in a pre-heated oven at 150 °C for 40 h. After cooling to room temperature at a rate of 5 °C min^{-1}, the single crystals of Ga-TCPP obtained were filtered and washed multiple times with DMF followed by methanol and kept in methanol overnight before filtering and drying at 80 °C overnight.

Synthesis of STA-27, $Sc_2(O)(H_2O)_2$TCPP

STA-27 was synthesised using a mixed solvent system of DMF, aqeous 3.5 M HNO_3 and acetonitrile with $ScCl_3.6H_2O$ and H_4TCPP as the precursors. 232.4 mg $ScCl_3.6H_2O$ (0.895 mmol) and 41.2 mg TCPP (0.074 mmol) were weighed out into a Teflon-liner (total volume ~30 mL) equipped with a magnetic stirrer bar. 7.5 mL of DMF followed by 7.5 mL of 3.5 M aq. HNO_3 and 7.5 mL acetonitrile were added to the mixture using either a syringe or measuring cylinder. The solution was stirred at room temperature until the colour of the solution changed to pale yellow (usually 45-50 min). The stirrer bar was removed, and the Teflon-liner was placed inside a stainless-steel autoclave before heating in a pre-heated oven at 150 °C for 30 h. After cooling to room temperature at a rate of 5 °C min^{-1}, lozenge shaped single-crystals of STA-27 were obtained. The crystals were washed multiple times with DMF and methanol and kept in methanol overnight before filtering and drying at 80 °C overnight. CHN analysis : Calc. C, 49.33; H, 3.42; N, 5.49 wt%. Meas. C, 49.37; H, 3.33; N, 5.49 wt%.

View Article Online
DOI: 10.1039/C8TA10610J

Catalysis

3.1 Conjugate addition of 2-methylindole to methyl vinyl ketone

1 mmol of 2-methylindole, 1 mmol of methyl vinyl ketone, 0.5 mmol of 1-methylnaphthalene and 1.5 mol % of STA-27 (or MIL-100(Sc)) were added to 5 mL DCM and stirred at room temperature for 8 h under an inert atmosphere. After the reaction, the reaction mixture was filtered and washed multiple times with a minimum amount of water. The product was extracted using DCM and dried over $MgSO_4$. After the removal of DCM under vacuum, the crude product obtained was purified by flash chromatography using hexane: ethyl acetate (4:1) eluent. The pure product, 4-(2-methyl-1H-indol-3-yl)butan-2-one was obtained as a yellow liquid which yields a white solid when kept undisturbed. Isolated yield = 66 % (0.06 mmol). ^{1}H NMR (400MHz, $CDCl_3$): 7.81 (s, 1H), 7.52 (m, 1H), 7.29 (m, 1H), 7.13 (m, 2H), 3.0 (t, 2H, J = 7.8 Hz), 2.80 (t, 2H, J = 7.7 Hz), 2.41 (s, 3H), 2.14 (s, 3H). ^{13}C NMR (75 MHz, $CDCl_3$): 209.1 (C-O), 135.3 (Ar-C), 131.2 (Ar-C), 128.3 (Ar-C), 121.0 (Ar-CH), 119.2 (Ar-CH), 117.8 (Ar-CH), 110.5 (Ar-CH), 110.3 (ArCH-CH_2), 44.3 (CH_2), 30.3(CH_3), 18. 4(CH_2), 11.7 (CH_3). HRMS (EI+) Calculated: 202.122; Obtained: 202.126. Data in accordance with the literature.[12e]

3.2 Imine condensation between 4’-fluoroacetophenone and benzyl amine

1 mmol of 4’-fluoroacetophenone, 1 mmol of benzylamine, 0.5 mmol of 1-methylnaphthalene and 1.5 mol % of STA-27 (or MIL-100(Sc)) were added to 5 mL toluene and heated at 90 °C for 24 h under an inert atmosphere. After the reaction, the reaction mixture was diluted using minimum amount of toluene and filtered through Na_2SO_4. The filtrate was washed with 0.1 M HCl solution and concentrated under vacuum to obtain the pure product as a yellowish-brown oil. Isolated yield = 75 % (0.48 mmol). ^{1}H NMR (400MHz, $CDCl_3$): 7.90 (ddd, 2H, J = 8.4, J = 5.2, J= 2.6), 7.39 (m, 6H), 7.10 (m, 2H), 4.76 (s, 2H), 2.35 (s, 3H). ^{13}C NMR (75 MHz, $CDCl_3$): 163.8 (ArC-F, J = 249 Hz), 164.7 (C=N), 140.4 (ArC), 137.1 (ArC, J = 3.0 Hz), 128.7 (2xArCH, J = 8.3 Hz), 128.45 (2xArCH), 127.7 (2xArCH), 126.5 (ArCH), 115.0 (2×ArCH, J = 21 Hz), 55.7 (CH_2), 15.8 (CH_3). HRMS (EI+) Calculated: 228.118; Obtained: 228.122. Data in accordance with the literature.[12e]

3.3 Carbonyl ene reaction between ethyl trifluoropyruvate and α-methylstyrene

View Article Online
DOI: 10.1039/C8TA10610J

2.25 mmol of ethyl trifluoropyruvate, 2.7 mmol of α-methylstyrene, 0.5 mmol of 1-methylnaphthalene and 1.5 mol% of STA-27 (or MIL-100(Sc)) were added to 5 mL toluene and stirred at room temperature for 6 h under inert atmosphere. After the reaction, the reaction mixture was filtered and concentrated under vacuum, the crude product obtained was purified by flash chromatography using hexane: ethyl acetate (6:1) eluent. The pure product, ethyl-2-hydroxy-4-phenyl-2-trifluoromethyl)pent-4-enoate, was obtained as a pale liquid. Isolated yield = 60 % (1.3 mmol). ^{1}H NMR (400MHz, $CDCl_3$): 7.34 (m, 5H), 5.42 (s, 1H), 5.32 (s, 1H), 4.06 (dq, 1H, *J* = 10.6 Hz, 7.0Hz), 3.65 (dq, 1H, *J* = 10.6 Hz, 7.0Hz), 3.33(d, 1H, J = 14.1 Hz), 3.08 (d, 1H, J = 14.1Hz), 1.14 (t, 3H, 7.0Hz). ^{19}F NMR (282 MHz, $CDCl_3$): -78.4. ^{13}C NMR (75 MHz, $CDCl_3$): 168.7 (C=O), 140.8 ($C=CH_2$), 128.0 (ArC), 127.5 (2xArCH), 126.6 (ArCH), 124.3 (2xArCH), 122.3 ($CH_2=C$), 119.3 (C-OH), 63.3 (CH_2), 36.8 (CH_2), 13.3 (CH_3). HRMS (EI+) Calculated: 289.273; Obtained: 289.276. Data in accordance with the literature.[12e]

Characterisation

Powder X-ray diffraction (PXRD) patterns on finely ground MOF samples were collected in Debye-Scherrer geometry on Stoe STADI P diffractometers with primary monochromation (Cu $K_{\alpha 1}$, λ = 1.54056 Å), using either 0.5- or 0.7-mm glass capillaries. Variable temperature PXRD (VT-PXRD) measurements for STA-27 were performed in open quartz capillaries in a flow of dry nitrogen flow with a ramp rate of 5 °C min^{-1} and held at the desired temperature for 10 min prior to measurements. Data were collected from 25 to 225 °C and after cooling down to 25 °C using a Cobra Plus non-liquid-nitrogen cryostream (Oxford Cryosystems).

Single crystal X-ray diffraction data for $Ga_2(OH)_2$TCPP were collected at 93 K using a Rigaku FR-X Ultrahigh Brilliance Microfocus RA generator/confocal optics with XtaLAB P200 diffractometer [Mo Kα radiation (λ = 0.71075 Å)]. Intensity data were collected using ω steps accumulating area detector images spanning at least a hemisphere of reciprocal space. Data for STA-27 and STA-27-*C* were collected at 173 K using a Rigaku MM-007HF High Brilliance RA generator/confocal optics with XtaLAB P100 diffractometer [Cu K_{α} radiation (λ = 1.54187 Å)]. Intensity data were collected using both ω and ϕ steps accumulating area detector images spanning at least a hemisphere of reciprocal space. Data for all compounds analysed were collected and processed (including correction for Lorentz, polarization and

View Article Online
DOI: 10.1039/C8TA10610J

absorption) using CrystalClear[19] or CrysAlisPro.[20] Structures were solved by dual-space methods (SHELXT),[21] and refined by full-matrix least-squares against F^2 (SHELXL-2018/2).[22] Non-hydrogen atoms were refined anisotropically, and aryl hydrogen atoms were refined using a riding model. Hydroxyl hydrogen atoms in $Ga_2(OH)_2$TCPP were located from the difference Fourier map and refined isotropically, subject to a distance restraint. Terminal oxygen atoms in STA-27 were identified as water molecules, although hydrogen atoms could not be located. STA-27-*C* showed extremely weak diffraction at higher angles and broadening of some diffraction spots. This led to the high values of R_{int} and other metrics but did not prevent the unambiguous determination of the structure of the MOF apart from the bridging species, which we tentatively assign as HCO_3^-. The data for STA-27 showed non-merohedral twinning (twin law 1 0 0.313 0 -1 0 0 0 -1, twin fraction 47 %), which was accounted for in the refinement. All three structures structure showed high proportions of void space ($Ga_2(OH)_2$TCPP: 856 Å^3, STA-27: 1069 Å^3, STA-27-*C*: 817 Å^3) and the SQUEEZE[23] routine implemented in PLATON[24] was used to remove the contribution of the disordered electron density in the void spaces. All calculations except SQUEEZE were performed using the CrystalStructure[25] interface. Selected crystallographic data are presented in Table 1. CCDC 1875994-1875996 contains the supplementary crystallographic data for this paper. The data can be obtained free of charge from The Cambridge Crystallographic Data Centre via www.ccdc.cam.ac.uk/structures. The topological analysis was carried out with the package ToposPro.[26]

Solid-state NMR (SS-NMR) spectra were recorded using a Bruker Avance III spectrometer equipped with a 9.4 T superconducting magnet (Larmor frequencies of 400.1 MHz for ^1H, 100.6 MHz for ^{13}C and 97.2 MHz for ^{45}Sc). Samples were packed into standard ZrO_2 rotors with outer diameters of 4 mm and rotated at the magic angle at a rate of 12.5 kHz (^{13}C) or 14 kHz (^{45}Sc, ^{27}Al). The ^{13}C NMR spectrum was recorded with cross polarisation (CP) from ^1H with a contact pulse (ramped for ^1H) of 2 ms. Signal averaging was carried out for 4096 transients with a recycle interval of 3 s. Two-pulse phase modulation (TPPM) decoupling of ^1H ($n_1 \approx 100$ kHz) was carried out during acquisition. For the ^{27}Al NMR spectra, signal averaging was carried out for 4096 transients with a recycle interval of 0.25 s. A rotor-synchronised x-2x spin echo pulse sequence was used with an echo delay of 71.43 µs and pulses of 1 and 2 µs (inherent flip angles of ≈ 36 and 72°). Signal averaging was carried out for 120 transients for each of 128 t_1 increments of 71.43 µs with a recycle interval of 0.25 s.

For the ^{45}Sc NMR spectra, signal averaging was carried out for 1024 transients with a recycle interval of 0.25 s. Both ^{27}Al and ^{45}Sc multiple-quantum (MQ) magic angle spinning (MAS) spectrum was recorded using a z-filtered pulse sequence and then sheared and referenced according to Pike *et al.*[27] For ^{45}Sc NMR spectra, signal averaging was carried out for 5664 transients for each of 20 t_1 increments of 35.7 ms with a recycle interval of 0.25 s. Chemical shifts are reported in ppm relative to TMS (^{13}C) or 0.06 M $Sc(NO_3)_3$ in D_2O (^{45}Sc), using L-alanine (**C**H_3 δ = 20.5 ppm) and $LaScO_3$ (δ= 162 ppm) as secondary solid references.

Thermogravimetric analysis (TGA) of all MOF samples was carried out on a Netzsch TGA 760 insrument for a temperature range of 20 - 800 °C at a heating rate of 5 °C min^{-1} in a continuous air flow. N_2 adsorption isotherms for all the MOFs were measured volumetrically on a Micrometrics Tristar at -196 °C. The CO_2 adsorptions isotherms were measured gravimetrically on Hiden IGA porosimeter at room temperature. All samples were activated at 150 °C prior to measurements.

The FTIR spectra were recorded with Nicolet Avatar 360 and Nicolet 6700 FTIR spectrometers accumulating 64 scans at a spectral resolution of 2 cm^{-1} and accuracy of 0.01 cm^{-1}. The IR measurements of STA-27 were made with (i) MOF samples spread on the surface of preliminary pressed KBr discs and (ii) self-supporting pellets. The pellets were treated directly in a specially designed IR cell allowing measurements at ambient and low (100 K) temperatures. The cell was directly connected to a vacuum-adsorption apparatus with a residual pressure lower than 10^{-3} Pa. The IR experiments were made *in situ* with as-prepared (air exposed) samples and samples activated by outgassing under high vacuum (~ 10^{-6} mbar) at ambient and elevated temperatures.

Grand canonical Monte Carlo simulations were carried out using the general-purpose molecular simulation code MuSiC.[28] The Lennard-Jones (LJ) parameters for the framework atoms were taken from the Dreiding forcefield,[29] with the exception of scandium, the parameters for which were taken from the Universal forcefield.[30] Dinitrogen LJ parameters were taken from the Transferable Potentials for Phase Equilibria (TraPPE) forcefield.[31] Lorentz-Berthelot mixing rules were applied for LJ interactions between different atom types, and interactions between atoms separated by a distance greater than the cut-off radius of 18 Å were truncated. GCMC moves implemented on the N_2 molecules (insertion, deletion, translation and rotation) were carried out with equal weighting. For each pressure point, 10 million iterations were used, 40 % of which were used for equilibration.

View Article Online
DOI: 10.1039/C8TA10610J

Table 1. Crystallographic data for $Ga_2(OH)_2TCPP$, STA-27 and STA-27-*C*

Parameter	$Ga_2(OH)_2TCPP$	STA-27	STA-27-*C*
Formula	$C_{32}H_{18}N_2O_{10}Ga_2$	$C_{32}H_{20}N_2O_{11}Sc_2$	$C_{34}H_{18}N_2O_{14}Sc_2$
Formula weight/g mol^{-1}	695.91	698.42	768.43
Temperature/K	93	173	173
Crystal System	Orthorhombic	Monoclinic	Orthorhombic
Space group	*Cmmm*	*P2/c*	*Pmna*
a/Å	6.68115(16)	15.504(7)	32.741(4)
b/Å	21.2861(4)	9.443(4)	7.797(3)
c/Å	15.9030(3)	15.975(7)	8.763(3)
β/°	-	99.277(14)	-
V/Å	2261.66(8)	2308.2(18)	2237.0(12)
Z	2	2	2
ρ(calcd) g cm^{-3}	1.072	1.005	1.141
Radiation type	Mo Kα	Cu Kα	Cu Kα
μ mm^{-1}	1.233	2.910	3.090
F(000)	732	712	780
Rint	0.0219	0.1396	0.5507
GOF	1.120	1.560	0.968
Final R1 values [I>2σ(I)]^a	0.0316	0.1409	0.1479
Final wR2 values (all data)^b	0.0958	0.4218	0.4332

Results and Discussion

Inspired by the synthesis conditions employed for isoreticular Al-*soc*-MOFs by Alezi *et al.*[10d] using a tetracarboxylic acid, the optimised solvothermal crystallisations (Table 2) in DMF and 3.5 M aq. HNO_3 using H_4TCPP and either $Al(NO_3)_3.9H_2O$ ($AlCl_3.6H_2O$) or $Ga(NO_3)_3.6H_2O$ as metal sources gave products containing crystalline $Al_2(OH)_2TCPP$ or $Ga_2(OH)_2TCPP$, respectively (Figures S1, S2).

View Article Online
DOI: 10.1039/C8TA10610J

Table 2: Optimising synthesis conditions for $Al_2(OH)_2TCPP$ and $Ga_2(OH)_2TCPP$. In each case 0.074 mmol of H_4TCPP was used, plus either 0.895 mmol of Al precursor (M:L = 12:1) or 0.628 mmol of Ga precursor (M:L = 8:1), respectively.

Metal Source	DMF (mL)	HNO_3 (3.5 M) (mL)	CH_3CN (mL)	Temperature (°C)	Time (h)	Phase
$Al(NO_3)_3.9H_2O$	7.5	7.5	7.5	150	30	Unidentified phase
$Al(NO_3)_3.9H_2O$	7.5	-	-	150	30	Amorphous
$Al(NO_3)_3.9H_2O$	7.5	-	7.5	150	30	Poorly crystalline
$Al(NO_3)_3.9H_2O$	7.5	7.5	-	150	30	$Al_2(OH)_2TCPP$
$AlCl_3.6H_2O$	7.5	7.5	-	150	30	$Al_2(OH)_2TCPP$
$Ga(NO_3)_3.6H_2O$	7.5	7.5	-	150	16	Unidentified phase (I)
$Ga(NO_3)_3.6H_2O$	7.5	7.5	-	150	30	Unidentified phase (I)
$Ga(NO_3)_3.6H_2O$	7.5	7.5	-	150	35	$Ga_2(OH)_2TCPP$ + impurity
$Ga(NO_3)_3.6H_2O$	7.5	7.5	-	150	40	$Ga_2(OH)_2TCPP$ + minor imp.
$Ga(NO_3)_3.6H_2O$	7.5	7.5	-	150	48	$Ga_2(OH)_2TCPP$ + impurity
$Ga(NO_3)_3.6H_2O$	7.5	7.5	-	150	72	$Ga_2(OH)_2TCPP$ + Impurity
$Ga(NO_3)_3.6H_2O$	7.5	7.5	-	150	96	Unknown phase (II)

PXRD indicates the aluminium and gallium MOFs prepared using H_4TCPP are isostructural (Figure 2A). The aluminium phase was prepared as a microcrystalline powder, while the gallium phase was prepared as single crystals (with a minor amount of impurities) that were amenable to structure solution by single crystal diffraction.

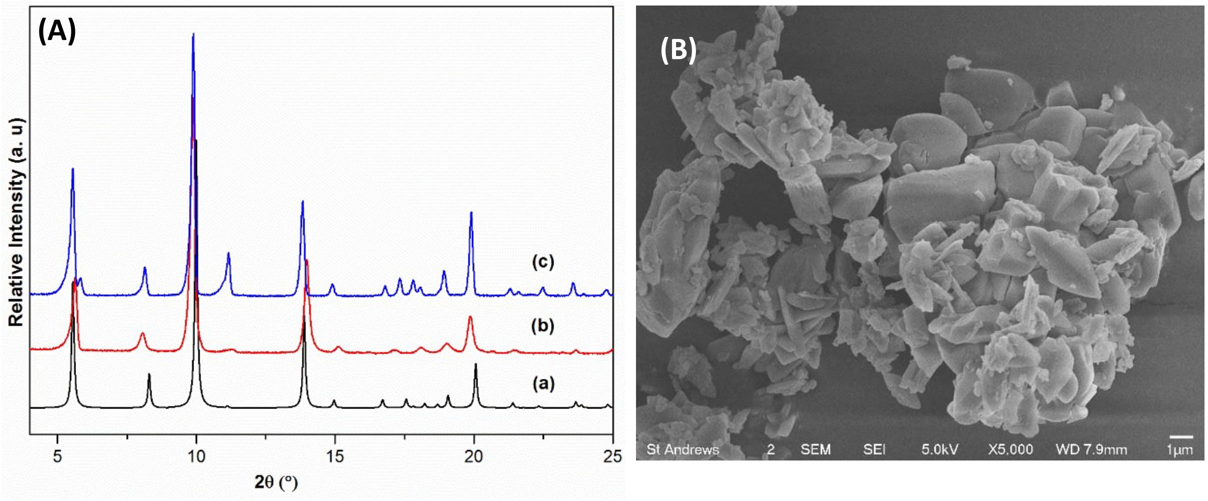

Figure 2 (A) Simulated pattern of (a) $Ga_2(OH)_2TCPP$ compared with the PXRD patterns of (b)as-synthesised $Al_2(OH)_2TCPP$ and (c) as-synthesised $Ga_2(OH)_2TCPP$ and (B) SEM image of $Al_2(OH)_2TCPP$.

View Article Online
DOI: 10.1039/C8TA10610J

The structure solution of $Ga_2(OH)_2$TCPP is described in the experimental section and Table 1 and the structure is illustrated in Figure 3. The Al and Ga TCPP MOFs are isostructural with $Al_2(OH)_2$TCPB reported by Krüger et al., the structure of which was solved from PXRD and computational modelling.[18] The difference between the TCPP and TCPB linkers is that in the former the CH groups of the central benzene ring in TCPB are replaced by N atoms (Scheme 1). In all these structures, the metal-based inorganic node is the infinite $MO_4(OH)_2$ chain of corner-sharing MO_6 octahedra linked by μ_2OH groups, similar to that found in the MIL-53 structure.[6] ^{27}Al MAS NMR and MQ (multiple-quantum) MASNMR of as-synthesised $Al_2(OH)_2$TCPP reveals a single resonance with a typical quadrapolar line shape (Figure 4A, Figure S3) similar to that observed for MIL-53(Al).[32]

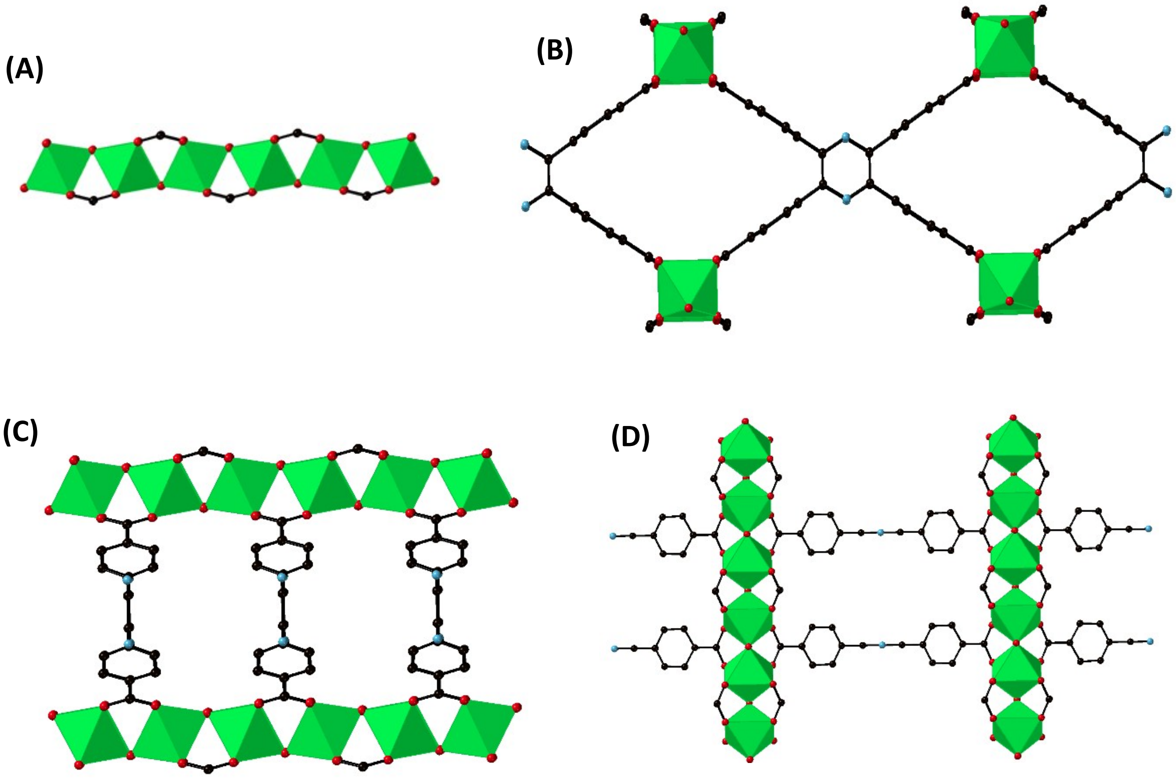

Figure 3 Crystal structure of $Ga_2(OH)_2$TCPP. A) 1D rod SBU comprising corner-sharing GaO_6 octahedra; $Ga_2(OH)_2$TCPP viewed along (B) the *z* axis; (C) the *x* axis and D) the *y* axis.. Hydrogen atoms are omitted for clarity. Colour codes: Ga, green; N, light blue; C, black; O, red. ($Al_2(OH)_2$TCPP is isostructural with $Ga_2(OH)_2$TCPP)

DOI: 10.1039/C8TA10610J

Although the $MO_4(OH)_2$ chain is the same type as that in MIL-53, the Al and Ga-TCPP MOFs here are rigid. Each chain is linked to eight others by the TCPP linkers, the carboxylate groups of which bridge adjacent metal cations in each chain. The four phenyl rings attached to the central pyrazine group are rotated at 90° to the plane of the pyrazine, planar with their carboxylate groups. Solid-state ^{13}C CP MAS NMR gives only a single resonance for each of the chemically distinct carbon atoms of the TCPP linker as expected from the crystal symmetry of the structure (Figure 4B).

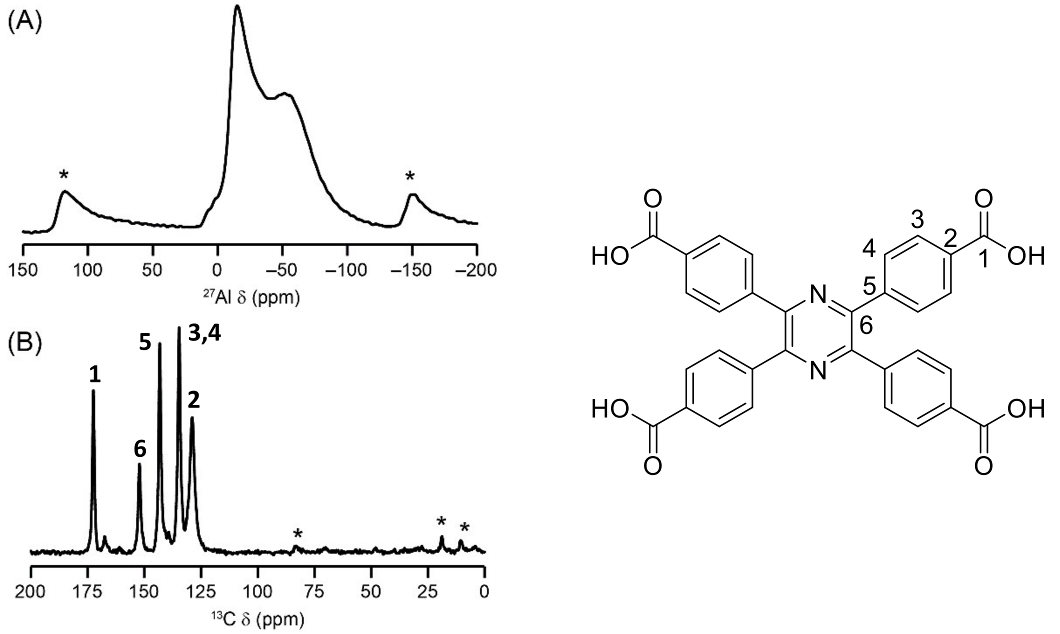

Figure 4 (A) ^{27}Al MAS NMR and (B) ^{13}C CP MAS NMR of $Al_2(OH)_2$TCPP. Peaks marked with asterisk are spinning side-bands. Assignment of ^{13}C peaks in B is shown in scheme (right).

Comparison of the experimental PXRDs of our materials with those simulated from the single crystal structure of $Ga_2(OH)_2$TCPP indicates that the Al phase has been prepared pure while the Ga phase contains a small amount of an unidentified impurity (Figure 2A). SEM images of $Al_2(OH)_2$TCPP (Figure 2B) showed lenticular crystals while the gallium sample (Figure S4) showed crystallites of different shapes confirming the presence of impurity. We concentrated on measuring properties of the pure Al phase. Notably, the previously-reported $Al_2(OH)_2$TCPB preparations contained some pseudo-boehmite impurity in all cases as detected by ^{27}Al MAS NMR, which are not present in $Al_2(OH)_2$TCPP (Figure 4A, Figure S3).

TGA of as-synthesised samples of $Al_2(OH)_2TCPP$ carried out in air indicated an initial weight loss of 26 % attributed to the loss of adsorbed solvent molecules from the pores. The framework was found to be stable up to 500 °C before linker degradation leads to structural disintegration (Figure 5A). N_2 adsorption at -196 °C gave a type I isotherm (Figure 5B), as predicted from the structure, with an uptake at $p/p^o = 0.1$ of 12.4 mmol g^{-1} (corresponding to a pore volume of 0.43 cm^3 g^{-1}) and a BET surface area of 1136 m^2 g^{-1}. This compares well with the 1118 m^2 g^{-1} (pore volume of 0.43 cm^3 g^{-1}) corrected specific surface area for the $Al_2(OH)_2TCPB$ phase by Krüger et al. after taking the boehmite impurity in that preparation into account.[18]

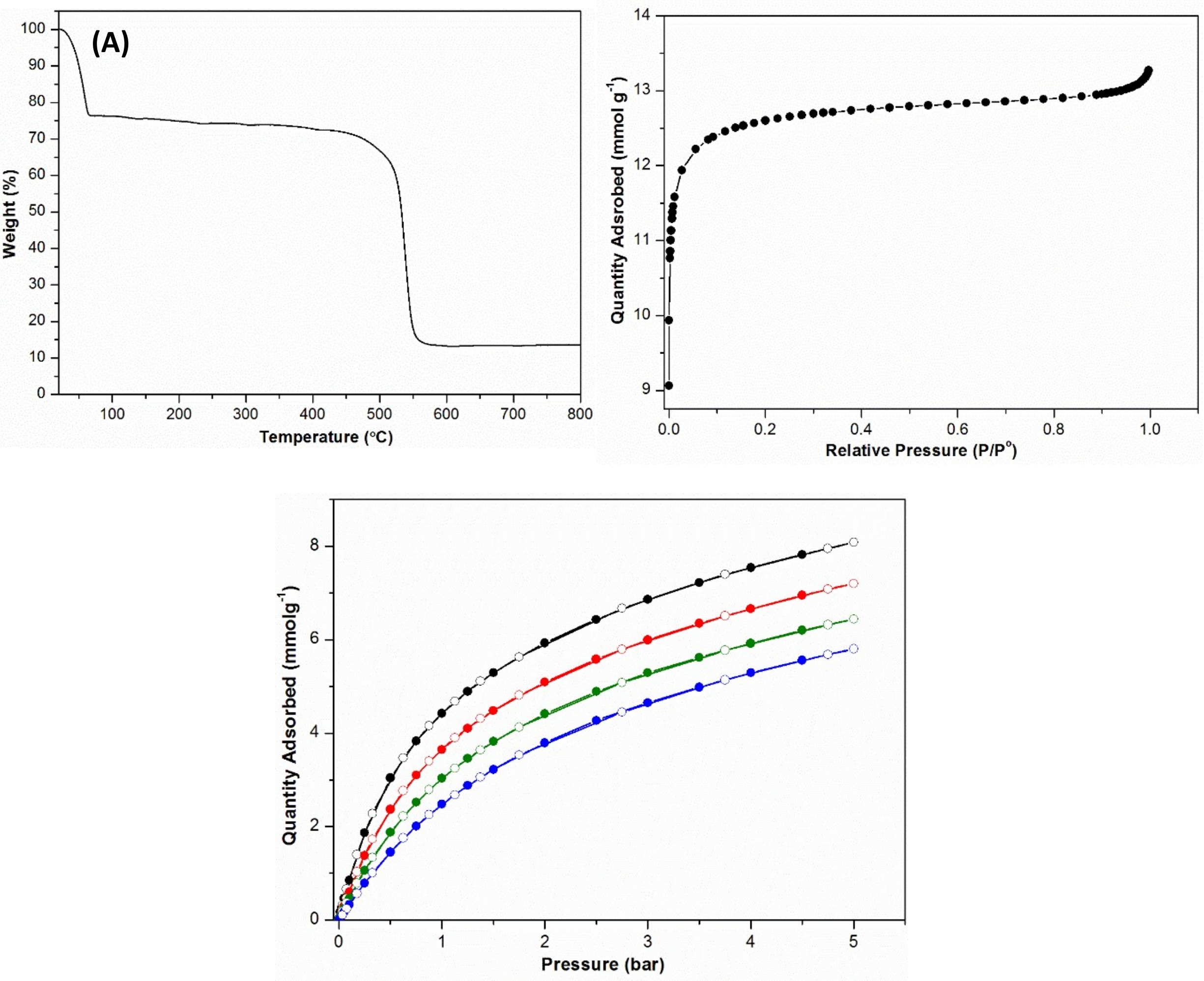

Figure 5 (A) TGA, (B) N_2 adsorption isotherm at -196 °C and (C) CO2 adsorption isotherms (black, 5 °C; red, 15 °C; green, 25°C; blue, 35°C) on $Al_2(OH)_2TCPP$.

The material was also investigated for its CO_2 uptake, because the availability and low toxicity of Al, the ease of synthesis of the linker and the presence of accessible hydroxyl and

View Article Online
DOI: 10.1039/C8TA10610J

amine groups of the MOF suggested potential application as a practical adsorbent. Variable-temperature CO_2 uptake studies of $Al_2(OH)_2$TCPP showed CO_2 uptake at 5 bar of 8.1 mmol g^{-1}, 7.2 mmol g^{-1} , 6.4 mmol g^{-1} and 5.8 mmol g^{-1} at 5 °C , 15 °C, 25 °C and 35 °C, respectively (Figure 5C). All of them showed full reversibility without hysteresis upon desorption. The uptake of CO_2 at 25 °C reached 3 mmol g^{-1} at 1 bar which is at the upper end of specific uptakes for MOFs without coordinatively unsaturated metal sites.[10d,33] (No CO_2 adsorption has been reported for $Al_2(OH)_2$TCPB)). $Al_2(OH)_2$TCPP was found to retain its crystallinity after N_2 and CO_2 adsorption by PXRD (Figure S5).

When moving to the Sc-TCPP synthesis system, employing the same metal:linker ratio, changing the metal source to $ScCl_3.6H_2O$ and varying the solvent mix did not give a scandium analogue of the $Al_2(OH)_2$(TCPP) and $Ga_2(OH)_2$(TCPP) phases reported above, but instead gave the distinct STA-27 phase under a relatively narrow set of conditions (Table ST1). Using $ScCl_3.6H_2O$ and H_4TCPP as precursors, with metal:linker ratio of 12:1 and a mixed solvent system of DMF, CH_3CN and 3.5 aq. HNO_3 (molar ratio Sc: H_4TCPP:DMF:CH_3CN:HNO_3 = 12:1:1311:1946:1608), heating at 150 °C gave phase-pure microcrystalline STA-27 after 16 h. Extending the heating time to 30 h gave lozenge-shaped single crystals of STA-27 suitable for structure solution by laboratory SCXRD (Figure 6A). The experimental PXRD pattern for the bulk sample of STA-27 showed good agreement with the pattern simulated from the solved structure, confirming its phase purity (Figure 6B).

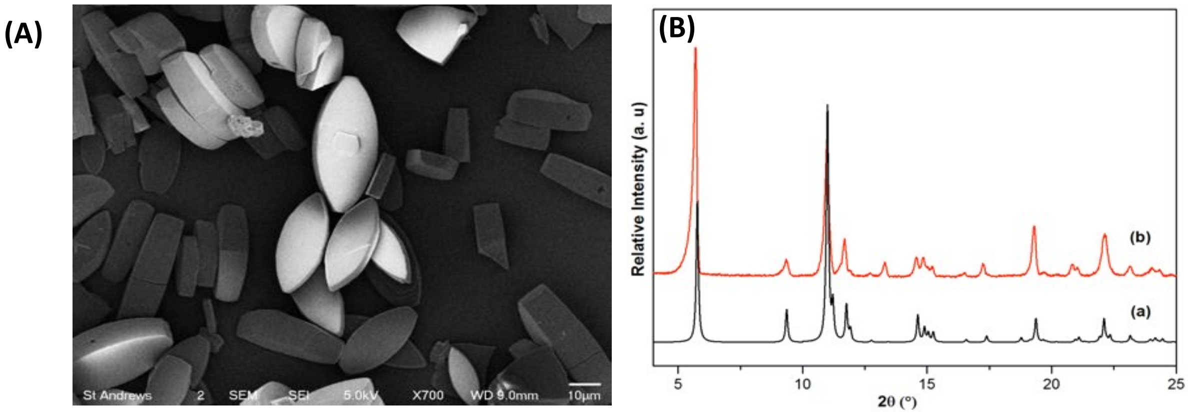

Figure 6 (A) SEM image of lozenge-shaped single crystals of STA-27. (B) (a) Simulated PXRD pattern of STA-27 compared with (b) the experimental pattern of as-synthesised STA-27.

STA-27 displays monoclinic crystal symmetry (*P*2/*c*, *a* =15.504(7) Å, *b* = 9.443(4) Å, *c* = 15.975(7) Å, β = 99.277°(14)) with infinite rods containing octahedrally-coordinated scandium cations running along the z axis, bridged by TCPP, giving rise to two different diamond-shaped channels parallel to the z axis (Figure 7). The rods are made up of Sc_2O_{11} dimers linked to one another via two carboxylate groups at each end (Figure 7). This definition of an infinite rod SBU containing carboxylate as well as O atoms linking metal cations is as described elsewhere.[34] Each Sc_2O_{11} dimer comprises two corner-sharing ScO_6 octahedra related by symmetry, the six O atoms of each of which include four from the TCPP linkers (Sc-O distances of 2.041 Å, 2.071 Å, 2.076 Å and 2.080 Å), one bridging μ_2O atom (Sc-O = 2.039 Å) and one O atoms of a terminal ligand (Sc-O = 2.097 Å). Notably, all these Sc-O distances are longer than those observed in $Ga_2(OH)_2$TCPP ((Ga-O bond distance of 1.983 Å and Ga-OH bond distance of 1.898 Å).

Charge balance requirements of the Sc_2O_{11} dimer suggest that if the μ_2O is unprotonated, the two terminal ligands are water molecules, giving an empirical formula of $Sc_2O(H_2O)_2$TCPP. Sc_2O_{11} units have been reported previously in the scandium succinate by Perles *et al.,*[35] where the Sc in each octahedron was coordinated to five carboxylate O atoms and a shared μ_2OH group, but in that case Sc cations in adjacent dimers are also connected by two succinate linkers. A similar rod-like SBU to that of STA-27 was reported for an actinide MOF[34,36] but not to our knowledge in transition or main group metal-based MOFs.

Each TCPP linker in STA-27 is bound to four different rod SBUs, when one set of diagonally opposite carboxylate groups of the linker connects the ScO_6 octahedra from different Sc_2O_{11} dimers to form two parallel rods, while the other set connects the dimers of different parallel rod building units. As a consequence, the benzoate groups of TCPP are rotated at 50° to its central planar pyrazine core. The resulting diamond-shaped channels of the structure are of two types, 1 and 2, of Figure 7. In type 1, the narrower dimension of its opening (3.9 Å free diameter) of the channel (viewed down z) separates dimers of two rods, while the wider dimension (10.8 Å free diameter) is between two pyrazine rings, while in the type 2 channels, the shorter distance (4.3 Å free diameter) is between the N atoms of pyrazine rings while the longer (8.2 Å free diameter) is between the Sc-based rods. Measured from the crystal structure, channels 1 and 2 are connected via narrow openings

View Article Online
DOI: 10.1039/C8TA10610J

of 2.5 Å while the openings between adjacent channels of type 2 are only 2 Å, but rotation of the relevant benzoate group phenyl rings could increase this. The channels are therefore 1D for most molecules.

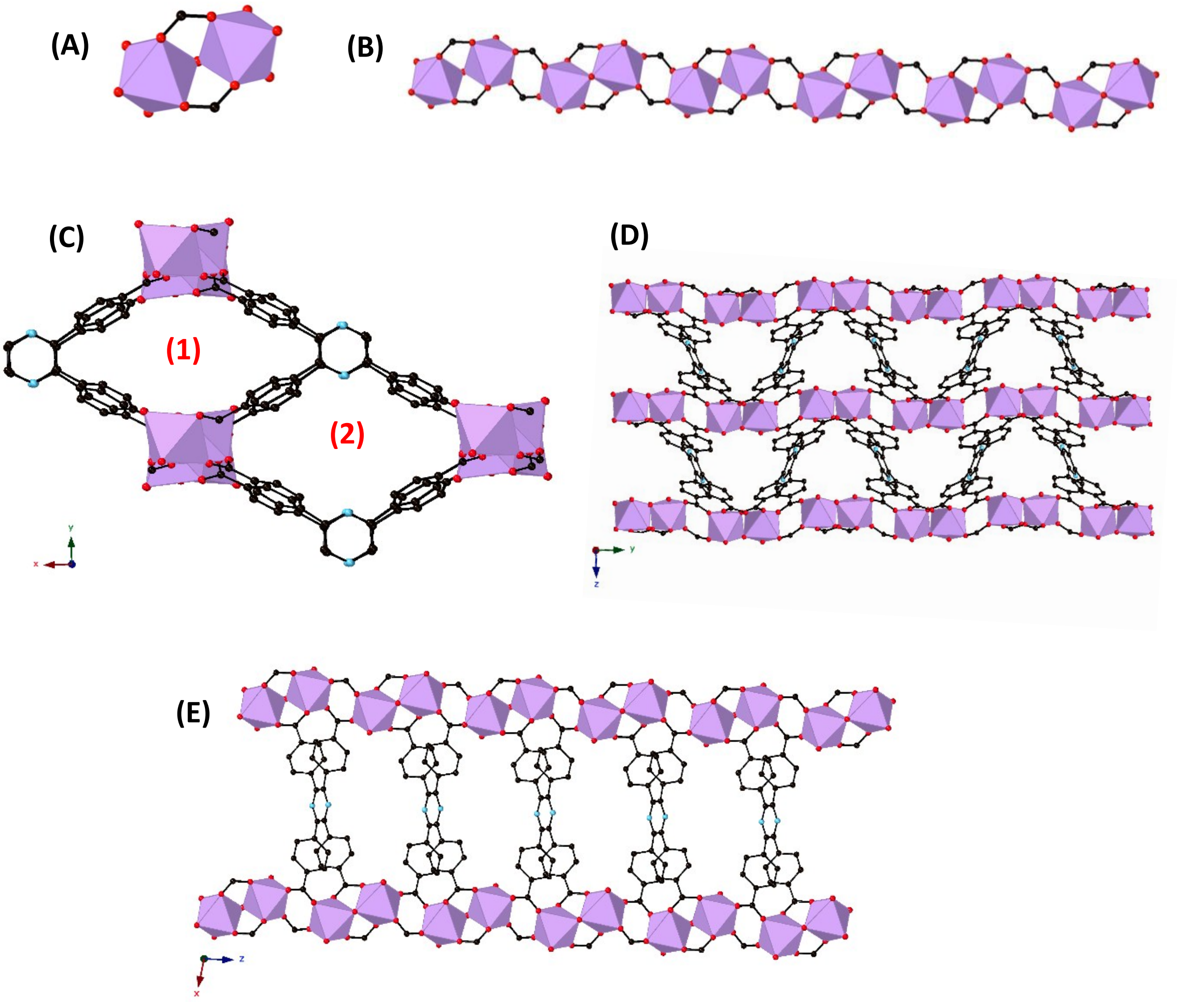

Figure 7 Crystal structure of STA-27. (A) Sc_2O_{11} dimer of STA-27, (B) 1D rod SBU of STA-27 made up of connected Sc_2O_{11} dimers, (C) two distinct diamond shaped pore channels of STA-27 viewed along the *z* axis, (D) STA-27 connected via TCPP viewed along *x* axis, (E) rod SBUs of STA-27 connected via TCPP viewed along *y* axis. Hydrogen atoms are omitted for clarity. Colour codes: Sc, lavender; N, light blue; C, black; O, red.

View Article Online
DOI: 10.1039/C8TA10610J

The determination of the topology of the underlying net in STA-27 is not as straightforward as it is for other MOFs with rod-like SBUs because there are several ways to deconstruct STA-27. According to the recommendations given by Schoedel *et al.* in a recent account on topology of the MOFs with rod SBUs,[34] the carboxylate carbon atoms should be considered as point of extensions to define the shape of the metal SBU. In STA-27, these nodes (all are symmetry-related to other) have three links within the rod SBU and one additional to the tetratopic 4-c linker which altogether give rise to a binodal (4,4)-c net, which can be derived from the binodal (4,5)-c sqc847 net of the EPINET project[37] via splitting the 5-c vertex into two 4-c vertices and modifying the bond sets accordingly which is accompanied with a symmetry reduction from *P*4/*mmm* and to *Pmma*. The deconstruction of STA-27 and the resulting net in its maximum symmetry embedding is visualized in Figure 8. Interestingly and in contrast to MIL-47, MIL-53 or MIL-71 the rod SBU in STA-27 does not form a zig-zag ladder but rather a sinoidal double-strand, highlighted in green in Figure 8D. STA-27 is the first MOF with this particular topology; to the best of our knowledge there is only one other framework compound, a ZMOF (Zeolitic Metal–Organic Framework), with an underlying topology that can also be derived from the sqc847 net, which builds also a binodal (4,4)-c net, however with a different set of edges and a different symmetry;[38] the net of this ZMOF can be found under the entry **zec** in the RCSR database.[39]

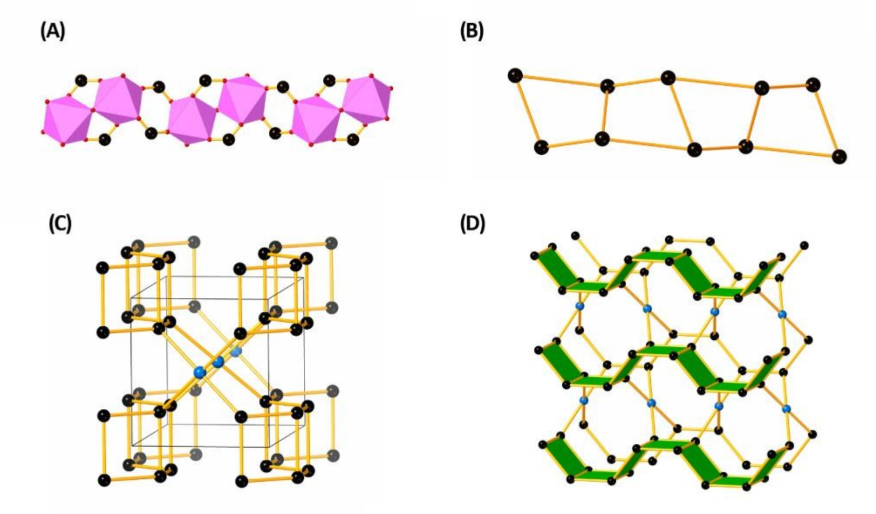

Figure 8: (A) Carboxylate carbon atoms (shown as larger black) spheres are taking as the points of extension, (B) which are the connected along the rod SBU, (C) giving rise to the binodal (4,4)-c net derived from the sqc847 net, (D) in the maximum symmetry-embedding the points of extension form a sinoidal double-strand, highlighted in green.

View Article Online
DOI: 10.1039/C8TA10610J

An alternative way of simplifying the structure of STA-27 into the underlying net is given by the straight-rod representation: In STA-27 there is only a single Sc atom all of which are bridged by carboxylate groups and each two of the bridging carboxylate carbon atoms point to the centre of an imaginary point lying almost exactly between two Sc atoms along the rods (Figure 9A). Connecting these midpoints leads to the binodal (4,4)-c net sqc969. Its representation with augmented linkers is shown in Figure 9B. From a rigorously mathematical perspective one could also argue that objects with infinite 1-periodic rods should be represented by a plane net, *i.e.* a rod packing. In this case the topology can be simply described with the 2-periodic binary 4-c net **sql** (**sql-b**): The rods have connections to four linkers in the plane and the linker links 4 rods (Figure 7C).

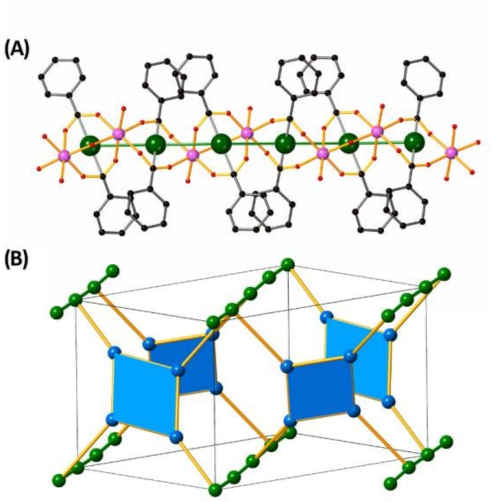

Figure 9: (A) Straight-rod representation of STA-27: Dummy atoms are placed between each two Sc atoms and (B) the final binodal (4,4)-c net sqc969 comprising of vertices along straight rods (green) and the linker which is represented in its augmented version (blue).

^{45}Sc is a 100% abundant nucleus (I=7/2) and so Sc MOFs can be analysed by ^{45}Sc MAS NMR to understand the Sc coordination enviornment.[12,14,15] The ^{45}Sc MAS NMR gives a single resonance with an isotropic chemical shift of 39 ppm (Figure 10) as determined by a combination of MQ MASNMR and peak shape matching, which is intermediate between the values of ScOH chains (δ = 55-62 ppm) and Sc_3O trimers (δ = 61-65 ppm) on the one hand and isolated ScO_6 octahedra (Sc_2BDC_3, δ = 4 ppm) on the other. A plot of the average quadrupolar product against isotropic chemical shift (Figure 10) distinguishes the local Sc environments according to their NMR characteristics (Figure S6).

View Article Online
DOI: 10.1039/C8TA10610J

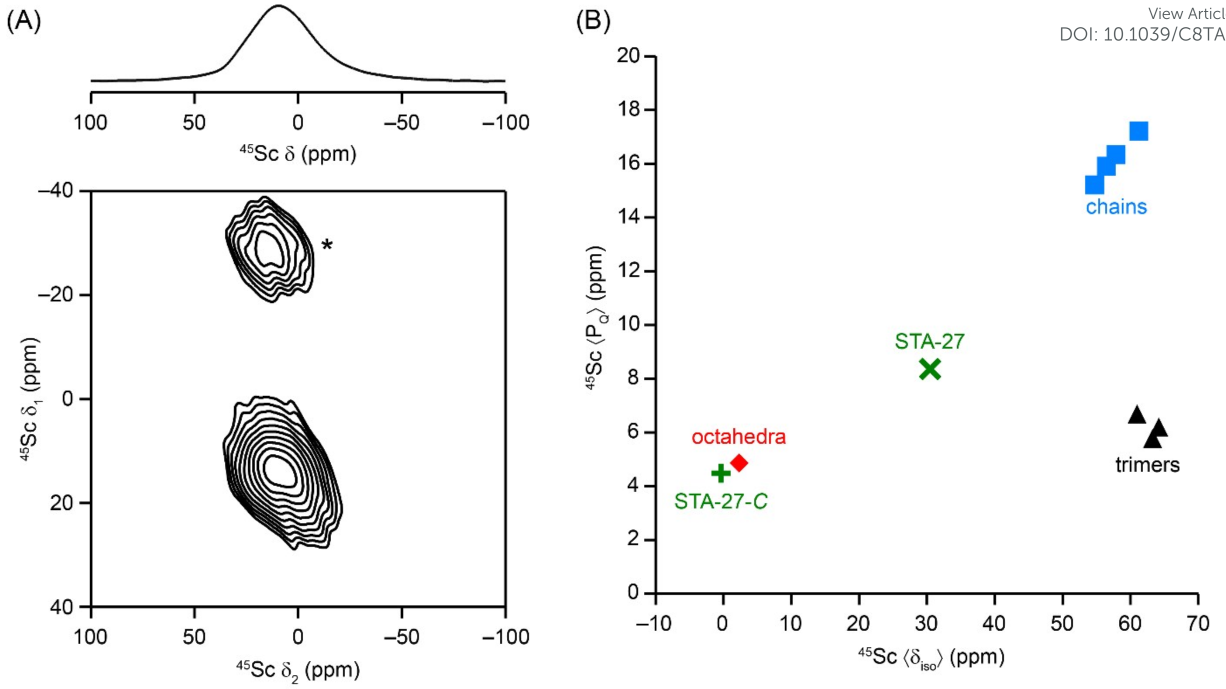

Figure 10 (A) ^{45}Sc MAS NMR and MQ MAS NMR spectra of STA-27 (asterisk denotes spinning side-band) and (B) Plot of mean ^{45}Sc isotropic shift $<\delta_{iso}>$ and quadrupolar product $<P_Q>$ for a series of Sc-containing MOFs with different Sc coordination motifs.[40] Red diamond = isolated ScO_6 octahedra (Sc_2BDC_3 and derivatives), blue squares = chains of ScO_6 octahedra (MIL-53 and derivatives) and black triangles = trimers of ScO_6 octahedra (MIL-88, MIL-100 and Sc-ABTC, ABTC = 3,3´,5,5´-azobenzenetetracarboxylate). Points for STA-27 are shown in green before (×) and after (+) heating. Reference points were obtained from multiple-quantum (MQ) MAS experiments carried out at 20.0 T, whereas spectra for STA-27 were recorded at 9.4 T.

TGA of as-synthesised STA-27 showed an initial mass loss of 8% attributed to the simultaneous evaporation of solvent molecules residing in the pores and water molecules attached to the clusters. Another mass loss of 7% was observed around 150 °C to 200 °C corresponding to the removal of DMF from the pores and possibly water from the ScO_6 octahedra[41] (Figure 11).

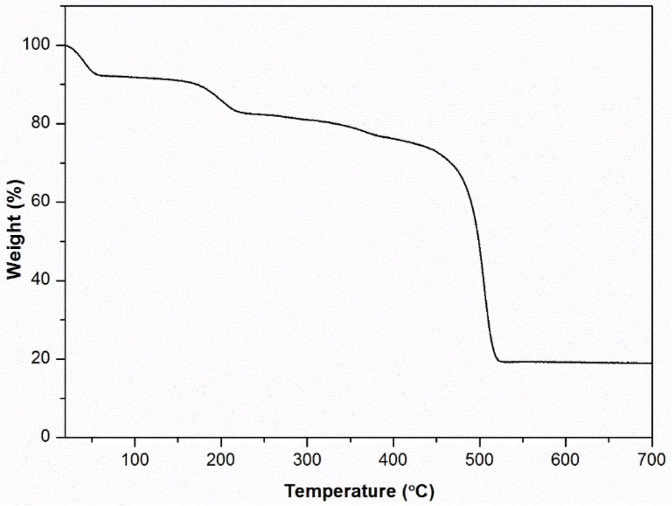

Figure 11 TGA of as-synthesised STA-27.

The response of STA-27 to heating was also studied by VT-PXRD and IR spectroscopy. VT-PXRD showed that STA-27 remained stable until 150 °C, above which a transformation to a second phase, displaying broader diffraction peaks, was observed (Figure 12).

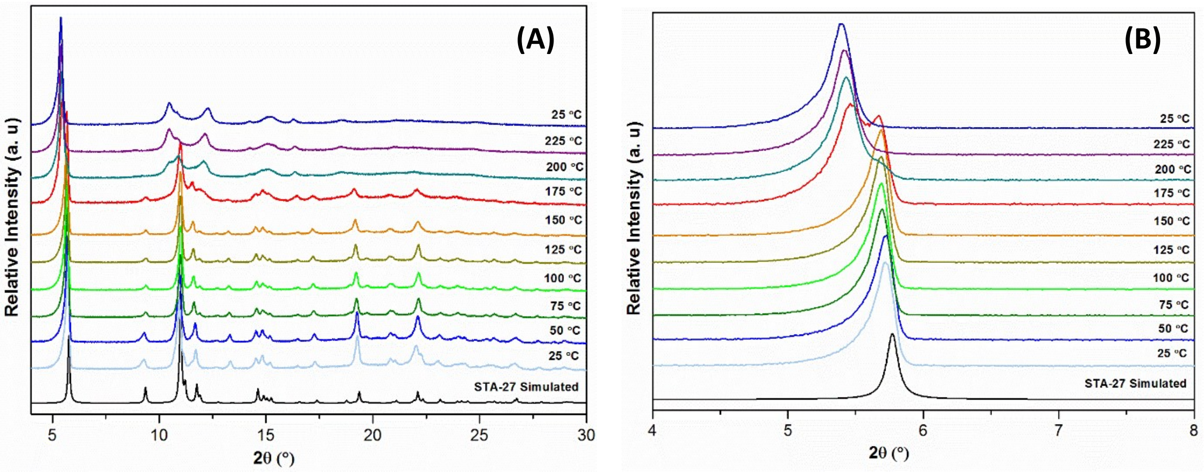

Figure 12 (A) VT-PXRD of STA-27 from 25 °C to 225 °C and cooled back to 25 °C. (B) Expanded low angle view of the PXRD patterns showing the change in peak positions after 175 °C.

IR measurements were performed heating the sample in vacuum up to 300 °C, at which temperature the STA-27 will have changed phase. Heating at 150 °C results in the removal of physically-bound water (broad absorbance centred around 3100 cm^{-1}) and the appearance of a band at 3669 cm^{-1}, which is attributed to the hydroxyl groups or isolated water molecules bound at Sc^{3+} sites (Figure 13A). Heating above this temperature results in

View Article Online
DOI: 10.1039/C8TA10610J

a decrease of the intensity of this band, as chemisorbed species are removed from the Sc^{3+} coordination sphere. Two probe molecules, CO (at -173 °C) and CD_3CN (at room temperature) were used to monitor the adsorption sites in STA-27 heated at different temperatures. For CO, a band at 2143 cm^{-1} that increases for sample heated to 150 °C and then decreases after heating at 200 °C is attributed to CO bound at hydroxyl groups (Figure 13B). These hydroxyls are of very low acidity as ν(OH) is shifted by -40 cm^{-1} upon CO adsorption (see the inset in Fig. 13B). For CD_3CN, bands at 2298 and 2277 cm^{-1} are assigned to CD_3CN binding at Sc^{3+} sites and a shoulder around 2270 cm^{-1} evidences interaction with OH groups. The fact that no Lewis acid sites were detected by CO indicates that CD_3CN displaces water molecules from the coordination sphere of scandium. Thus, IR spectroscopic studies showed the presence of Lewis acid sites and weak Brönsted sites upon heating the sample in vacuum at 150 °C, where the original STA-27 material is still stable (Figure 12).

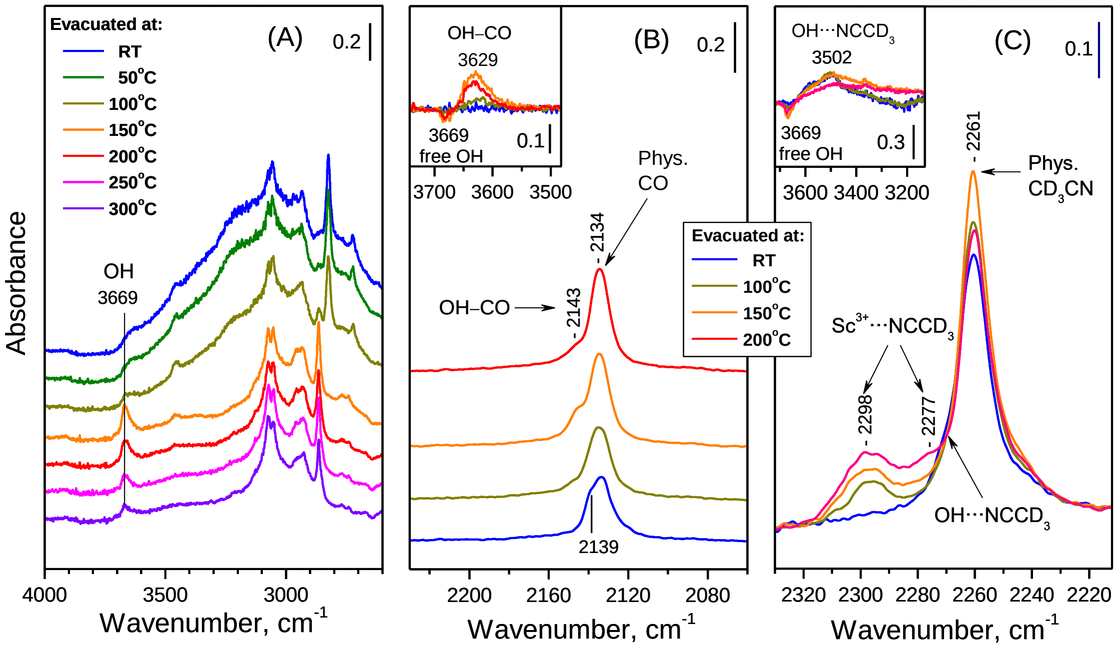

Figure 13 (A) IR spectra of STA-27 upon heating in vacuum at elevated temperatures. (B) IR spectra of CO adsorbed on the STA-27 sample pre-heated in vacuum at different temperatures. (C) IR spectra of STA-27 pre-heated in vacuum at different temperatures upon adsorption of CD_3CN showing the presence of coordinatively unsaturated metal sites.

N_2 and CO_2 gas adsorption was performed on a sample of STA-27 activated under vacuum at 150 °C to determine its permanent porosity. Moderate uptakes were achieved in each case (N_2, -196 °C, 0.1 bar, 8.2 mmol g^{-1}; CO_2, 25 °C, 1.6 mmol g^{-1} at 1 bar and 3.1 mmol g^{-1} at 5

View Article Online
DOI: 10.1039/C8TA10610J

bar; Figures 14A and 14B). The observed N_2 uptake of STA-27 was less than that predicted by Grand Canonical Monte Carlo (GCMC) simulation (10.5 mmol g^{-1} at 0.1 bar), suggesting some loss of accessible porosity upon heating and evacuation.

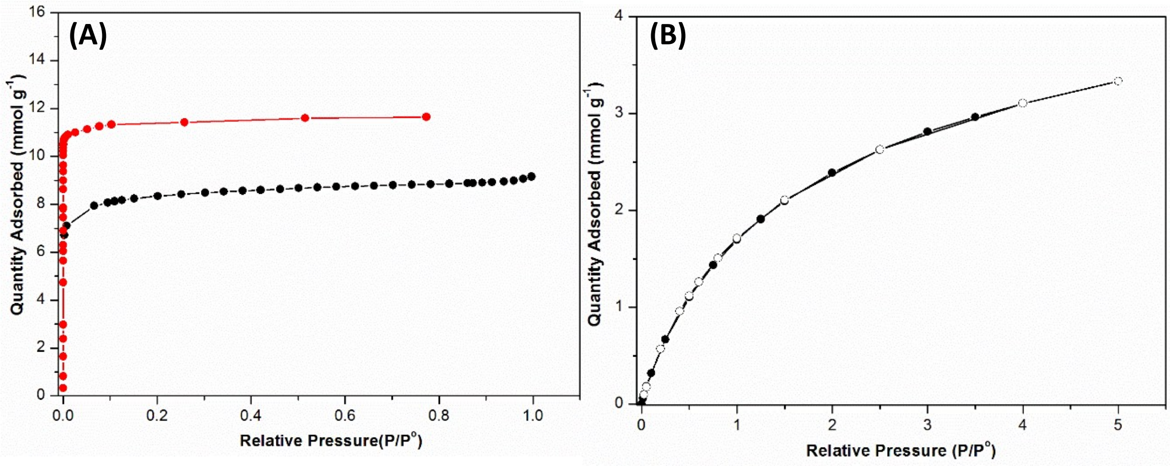

Figure 14 (A) N_2 adsorption isotherm at -196 °C for STA-27 (black) with the GCMC simulated isotherm from the crystal structure (red). (B) CO_2 adsorption isotherm at 25 °C for STA-27.

Single crystals obtained after heating STA-27 at 225 °C in N_2 and then being left to stand in laboratory air for 4 days showed uniform birefringence under crossed polars in the optical microscope (Figure 15A) and so were examined by SCXRD in spite of the broad peaks observed by PXRD (Figure 15B). Remarkably, despite the relatively low quality of the data, it was possible to obtain a crystal structure of this heated material, denoted STA-27-*C* (C for calcined), in the orthorhombic space group *Pmna* (Table 1, Figure 16). Projection of this structure down the z-axis shows the same arrangement of ScO_6 octahedra and TCPP linkers as the parent material, but there are important differences that are most clearly illustrated by views along the y-axis (Figure 16C). The ScO_6 octahedra in STA-27-*C* are isolated, linked along the z-axis by bridging carboxylate groups from the TCPP linkers. Each Sc^{3+} atom is still coordinated by four carboxylate O atoms and a terminal O ligand but the linking Sc-O-Sc atom is now replaced by two O atoms and the difference Fourier analysis reveals additional scattering between them. The exact nature of this species is unclear, but our model has a carbonate or bicarbonate species bridging adjacent Sc^{3+} cations, which we speculate forms upon exposure of the heated sample to air. The thermal decomposition of the scandium

View Article Online
DOI: 10.1039/C8TA10610J

dimer through breaking of the Sc-O-Sc linkage is unambiguous, however, and results in a phase change that is likely to be topotactic.

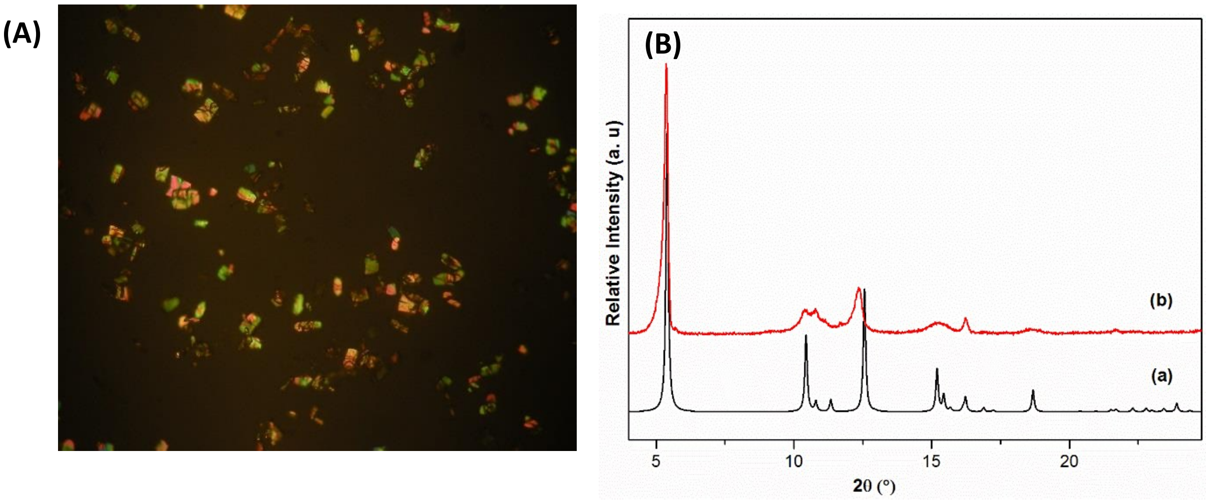

Figure 15 (A) Optical micrograph of crystals of STA-27-*C*. (B) (a) Simulated PXRD pattern of STA-27-*C* from single crystal structure compared with (b) pattern of STA-27-*C* after VT-PXRD.

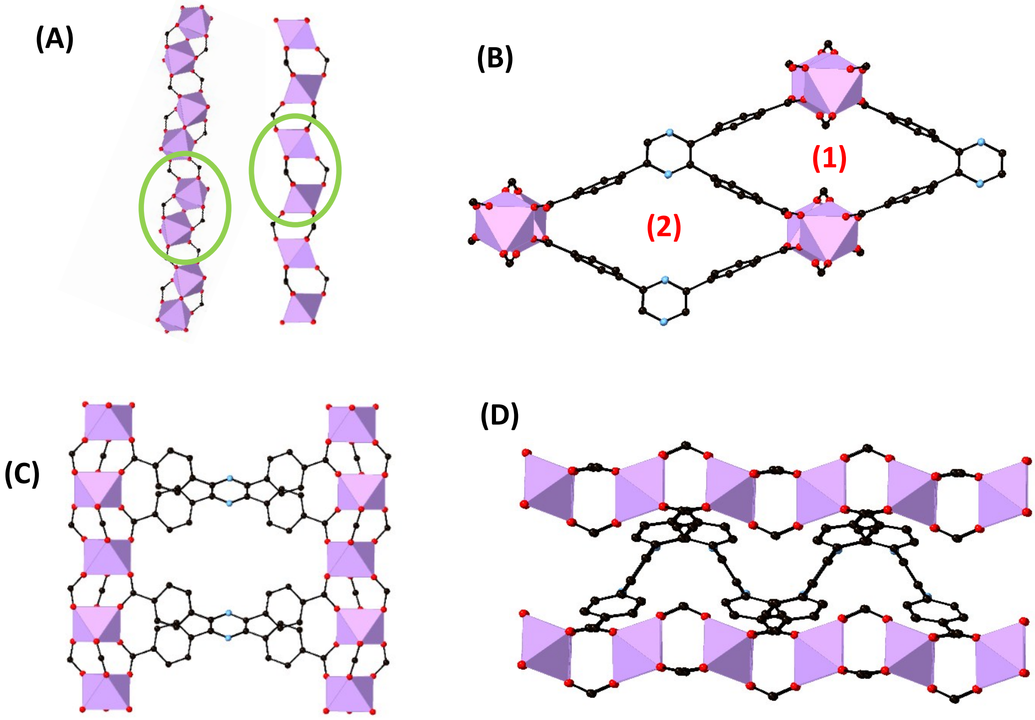

Figure 16 Crystal structure of STA-27-*C*. (A) 1D rod SBU of STA-27 (right) compared with the same of STA-27-*C* (left) the difference between the two SBUs are highlighted in the green sphere. (B) two distinct diamond shaped pore channels of STA-27-*C* viewed along the *z*-axis, (C) STA-27-*C* viewed along the *y*-axis and (D) STA-27-*C* viewed along the *x*-axis. Hydrogen atoms are omitted for clarity. Colour codes: Sc, lavender; N, light blue; C, black; O, red.

View Article Online
DOI: 10.1039/C8TA10610J

Further information on the transformation comes from ^{45}Sc MAS NMR (Figure 17). The heated sample shows two resonances, an intense sharp peak (δ_{iso} -50 ppm) together with a broad resonance of much lower intensity. Plotting the mean ^{45}Sc isotropic shift $<\delta_{iso}>$ and quadrupolar product $<P_Q>$ for STA-27 before and after heating along with those from a series of Sc MOFs with different Sc coordination (Figure 10), it was found that the value observed for the major peak of heated STA-27 was near to that of the isolated octahedra, in agreement with the structure indicated by SCXRD (Figure 16). N_2 adsorption of STA-27-*C* at -196 °C showed considerable reduction in porosity, which we attribute to the loss of crystallinity resulting from the phase transition (Figure S7). In addition to the characteristic peaks of TCPP, ^{13}C CP MAS NMR of STA-27-*C* shows a signal at 179 ppm, which might be assigned to carbonate or bicarbonate species similar to those reported previously at shifts of 168 – 171 ppm.[42]

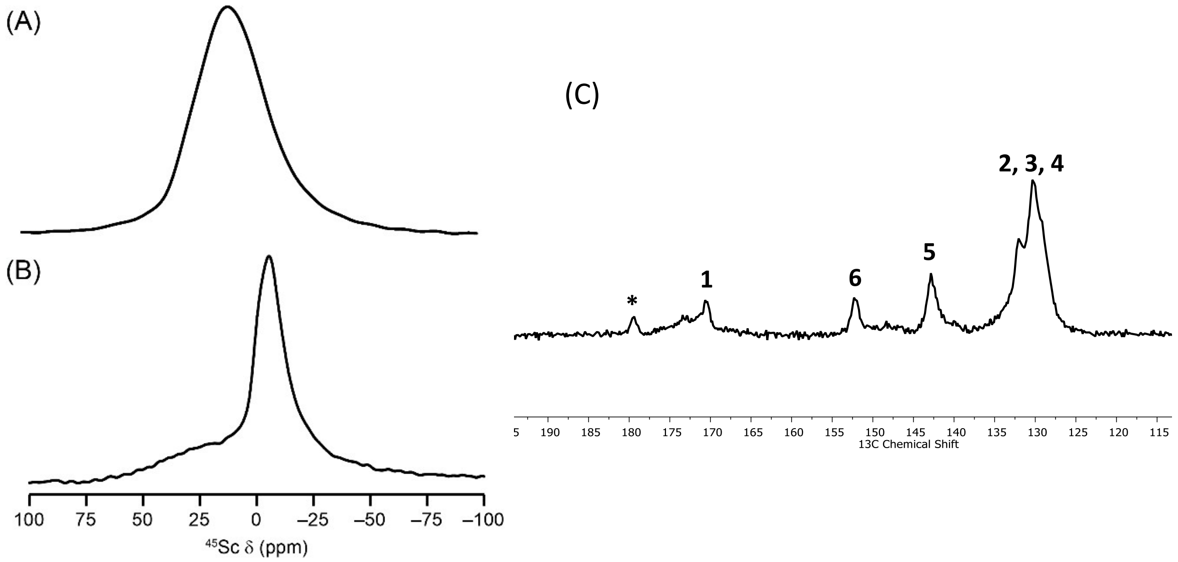

Figure 17 ^{45}Sc MAS NMR of (A) STA-27, (B) STA-27-*C* and (C) ^{13}C CP MAS NMR Of STA-27-*C.* Numbers on (C) corresponds to assignments to C atoms of TCPP as shown in Figure 4.

STA-27 pre-heated at 120 °C was found to be a highly active Lewis acidic catalyst for Friedel-Crafts Michael addition reactions, imine condensation and carbonyl ene reaction. Its performance is comparable with that of MIL-100(Sc) (Tables 3-5).[12d] STA-27 recovered after catalysis retained its crystallinity (Figure 18), and also retained its crystalline nature over five catalytic cycles when tested for imine condensation, with slight decrease in the catalytic

View Article Online
DOI: 10.1039/C8TA10610J

activity in each cycle (Figure S8). This loss in catalytic activity can be due to mass loss in repeated recycling and activation or due to substrate species occupying the pores.

Table 3: Conjugate addition of 2-methylindole to methyl vinyl ketone[a]

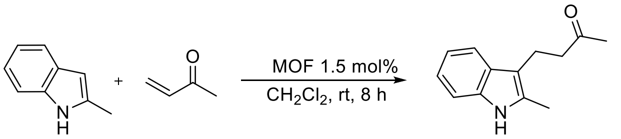

Entry	Catalyst	Product[b](%)
1	No Catalyst	2
2	STA-27	70
3	MIL-100(Sc)	74

[a] Reaction conditions: 1 mmol of 2-methylindole, 1 mmol of methyl vinyl ketone, 0.5 mmol of 1-methylnaphthalene and 1.5 mol% catalyst was added to 5 mL DCM and stirred at room temperature for 8 h. The mol% is calculated according to the molecular weight based on a formula unit containing one Sc-O cluster. [b] Conversion was determined by ^1H NMR using 1-methylnaphthalene as the internal standard.

Table 4: Imine condensation between 4'-fluoroacetophenone and benzylamine[a]

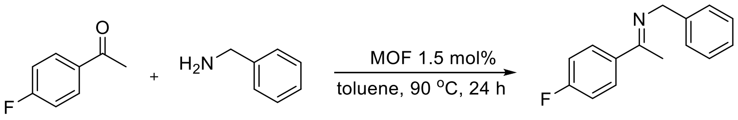

Entry	Catalyst	Product[b](%)
1	No Catalyst	2
2	STA-27	83
3	MIL-100(Sc)	80

[a]Reaction conditions: 1 mmol of 4'-fluoroacetophenone, 1.3 mmol of benzylamine, 0.5 mmol of 1-methylnaphthalene and 1.5 mol % catalyst was added to 5 mL toluene and heated at 90 °C for 24 h. [b] Conversion determined by ^1H NMR using 1-methylnaphthalene as internal standard.

View Article Online
DOI: 10.1039/C8TA10610J

Table 5: Carbonyl ene reaction between ethyl trifluoropyruvate and α-methylstyrene[a]

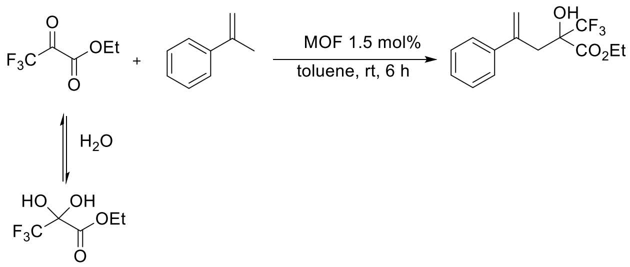

Entry	Catalyst	Product[b](%)
1	No Catalyst	2
2	STA-27	68
3	MIL-100(Sc)	75

[a] Reaction conditions: 2.25 mmol of ethyl trifluoropyruvate, 2.7 mmol of α-methylstyrene, 0.5 mmol of 1-methylnaphthalene and 1.5 mol % catalyst was added to 5 mL toluene and stirred at room temperature for 6 h. [b] Conversion determined by ^{1}H NMR using 1-methylnaphthalene as the internal standard.

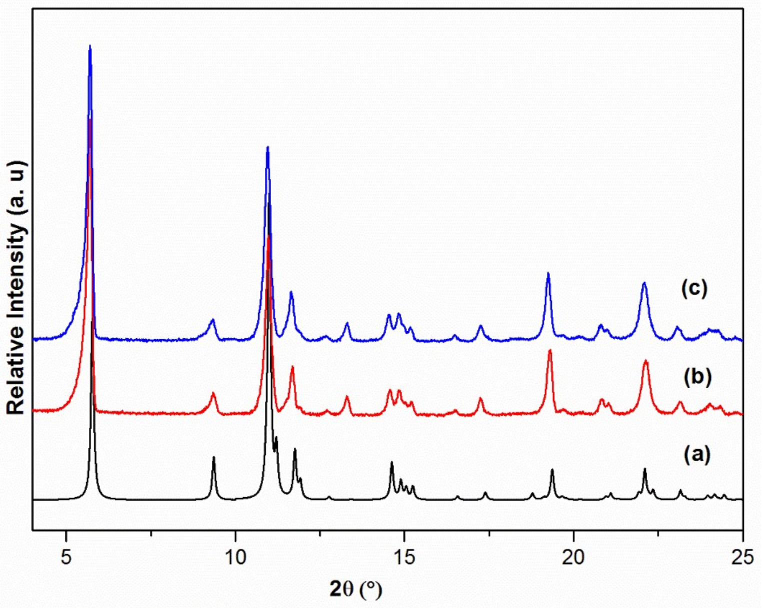

Figure 18 (a) Simulated pattern of STA-27 with the PXRD patterns of (b) STA-27 before catalysis and (c) STA-27 recovered after imine condensation reaction. STA-27 was filtered, washed multiple times with toluene followed by methanol before drying at 100 °C overnight prior to PXRD measurements.

To prove the heterogeneous nature of the catalyst, the MOF was filtered off 5 h into the imine condensation reaction of Table 4 while the solution was still hot, and the conversion measured (Figure S9, 41.5%,). The conversion in the solution was re-measured after a

View Article Online
DOI: 10.1039/C8TA10610J

further 7 h of heating (42.1%). That the conversion stays is so similar after the MOF was removed confirms the reaction is catalysed heterogeneously. Furthermore, after completion of the carbonyl-ene reaction between ethyl trifluoropyruvate and α-methylstyrene, STA-27 was recovered by removal of the reaction solution *via* syringe and N_2 adsorption and TGA were measured on the dried MOF. N_2 adsorption showed much lower uptake than for activated STA-27 (ca. 50%) and the TGA of the MOF showed the loss of residual organics above 100 °C (Figure S10). $^{19}F\{^1H\}$ NMR of dissolved MOF after N_2 porosimetry showed the characteristic peak of the product, ethyl-2-hydroxy-4-phenyl-2-trifluoromethyl)pent-4-enoate, at -78.4 ppm (Figure S11). The MOF was then filtered after being immersed in acetone overnight, washed multiple times with acetone, and dried. N_2 adsorption and TGA then show similar uptake and TGA trace to the original activated STA-27 (Figure S10). Taken together, these observations indicate that product is formed catalytically within, and can leave, the pores of the MOF.

In contrast to the high activity of STA-27, STA-27-*C* was found to have low activity for the Lewis acid catalysed reactions. For example, while STA-27 showed up to 83 % conversion in the imine condensation between 4’-fluoroacetophenone and benzylamine, STA-27-*C* showed only 36 %. The loss of crystallinity resulting from the phase transition presumably reduces the accessibility to potential Lewis acidic Sc^{3+} sites in the framework for substrate molecules, and hence decreases the catalytic activity of the MOF.

Conclusions

A series of MOFs has been prepared using trivalent metal cations of different ionic radii (Al^{3+}, Ga^{3+} and Sc^{3+}) and the tetracarboxylic acid H_4TCPP, which is readily formed via a two-step synthesis using inexpensive reagents. Al and Ga give $M_2(OH)_2TCPP$, which is isostructural to a previously reported $Al_2(OH)_2TCPB$, as might have been expected from the similarity of the linker. Investigation of the Al form shows that it is a thermally stable MOF which possesses a promising CO_2 adsorption performance.

Using $ScCl_3.6H_2O$ and H_4TCPP in a mixed solvent system of DMF, CH_3CN and 3.5 M aq. HNO_3 gives a new Sc MOF, STA-27. Unlike the Al and Ga forms, which possess a metal-based 1D rod SBU of infinite corner-sharing octahedra, STA-27 possesses a 1D rod SBU not observed previously in trivalent metal MOFs. In this rod, corner-sharing dimers of two ScO_6 octahedra (formula Sc_2O_{11}) are linked to give a MOF that possesses two distinct types of parallel diamond-shaped channels. The material is an active and reusable catalyst for organic C-C and C=N forming reactions: Sc^{3+} cations that have had water molecules displaced from their octahedral coordination shell are thought to be the active Lewis acid sites. The activity is comparable to that reported for the active Lewis acid catalyst MIL-100(Sc). Upon heating at 200 °C and above, STA-27 transforms to STA-27-*C*, in which the dimeric Sc_2O_{11} units present in the rods rearrange to isolated ScO_6 octahedra, as shown by X-ray diffraction and solid-state NMR. The topotactic transformation results in some loss of crystallinity and a reduction in pore volume and catalytic activity.

Acknowledgements

RRRP, MLC and PAW would like to thank the Engineering and Physical Sciences Research Council (EPSRC) and CRITICAT Centre for Doctoral Training for Financial Support [Ph.D. studentship to RRR; EP/L016419/1]. MML and PAW would also like to thank EPSRC for the FLEXICCS grant (Versatile Adsorption Process for the Capture of Carbon Dioxide from Industrial Sources; EP/N024613/1). KKC, MYM and KIH are grateful to the Bulgarian National Science Fund for the financial support (Contract no: DFNI T02/20). We thank Vladislav Blatov, Davide Proserpio, and Alexandrov Eugeny for helpful discussions regarding the topological analysis.

References

1 a) H. Furukawa, K. E. Cordova, M. O'Keeffe and O. M. Yaghi, *Science.*, 2013, **341**, 1230444; b) H. -C. Zhou, J. R. Long and O. M. Yaghi, *Chem. Rev.*, 2012, **112**, 673-674.

2 a) T. Loiseau, C. Volkringer, M. Haouas, F. Taulelle and G. Férey, *C. R. Chim.*, 2015, 18, 1350-1369; b) L. -H. Schilling, H. Reinsch and N. Stock, *The Chemistry of Metal-Organic Frameworks: Synthesis, Characterisation, and Applications*, *Wiley-VCH*, 2016, 105-135.

3 a) I. A. Lázaro, S. Haddad, S. Sacca, C. O. -Tavra, D. Fairen-Jimenez and R. S. Forgan, *Chem.*, 2017, **2**, 561-578; b) M. H. Teplensky, M. Fantham, P. Li, T. C. Wang, J. P.

View Article Online
DOI: 10.1039/C8TA10610J

Mehta, L. J. Young, P. Z. Moghadam, J. T. Hupp, O. K. Farha, C. F. Kaminski and D. F. - Jimenez, *J. Am. Chem. Soc.*, 2017, **139**, 7522-7532.

4 a) L. E. Kreno, K. Leong, O. K. Farha, M. Allendrof, R. P. Van Duyne and J. T. Hupp, *Chem. Rev.*, 2012, **112**, 1105-1125; b) M. G. Campbell, S. Liu, T. Swager and M. Dincá, *J. Am. Chem. Soc.*, 2015, **137**, 13780-13783.

5 a) J. Jiang and O. M. Yaghi, *Chem. Rev.*, 2015, **115**, 6966-6997; b) K. Manna, P. Ji, Z. Lin, F. X. Greene, A. Urban, N. C. Thacker and W. Lin, *Nature Communications.*, 2016, **7**, 1-11.

6 a) S. Bourrelly, P. L. Llewellyn, C. Serre, F. Millange, T. Loiseau and G. Férey, *J. Am. Chem. Soc.,* 2005, **127**, 13519-13521; b) C. Serre, F. Millange, C. Thouvenot, M. Noguès, G. Marsoller, D. Louër and G. Férey, *J. Am. Chem. Soc.*, 2002, **124**, 13519-13526; c) S. Couck, J. F. M. Denayer, G. V. Baron, T. Rémy, J. Gascon and F. Kapteijn, *J. Am. Chem. Soc*., 2009, **131**, 6326-6327; d) C. Volkringer, T. Loiseau, N. Guillou, G. Férey, E. Elkaïm and A. Vimont, *Dalton Trans*., 2009, **0**, 2241-2249.; e) T. Ahnfeldt, D. Gunzelmann, T. Loiseau, D. Hirsemann, J. Senker, G. Férey and N. Stock, *Inorg. Chem*., 2009, **48**, 3057-3064; f) F.–X. Coudert, A. U. Ortiz, V. Haigis, D. Bousquett, A. H. Fuchs, A. Ballandras, G. Weber, I. Bezverkhyy, N. Geoffroy, J.-P. Bellat, G. Ortiz, G. Chaplais, J. Patarin and A. Boutin, *J. Phys. Chem. C*., 2014, **118**, 5397-5405.

7 a) C. Serre, F. Millange, S. Surblé and G. Férey, *Angew. Chem. Int. Ed*., 2004, **43**, 6286-6289; b) S. Surblé, C. Serre, C. Mellot–Draznieks and G. Férey, *Chem. Commun*., 2006, **0**, 284-286; c) P. Horcajada, F. Salles, S. Wuttke, T. Devic, D. Heurtaux, G. Maurin, A. Vimont, M. Daturi, O. David, E. Magnier, N. Stock, Y. Filinchuk, D. Popov, C. Riekel, G. Férey and C. Serre*, J. Am. Chem. Soc*., 2011, **133**, 17839-17847.

8 a) P. Horcajada, S. Surblé, C. Serre, D.-Y. Hong, Y.-K. Seo, J. -S. Chang, J.–M. Grenéche, I. Margiolaki and G. Férey, *Chem. Commun*., 2007, **0**, 2820-2822; b) G. Férey, C. M. - Draznieks, C. Serre, F. Millange, J. Dutour, S. Surblé and I. Margiolaki, *Science*., 2005, **309**, 2040-2042; c) M. Latroche, S. Surblé, C. Serre, C. Mellot-Draznieks, P. L. Llewellyn, J. H. Lee, J.–San. Chang, S. H. Jhung and G. Férey, *Angew. Chem*., 2006, **118**, 8407-8411; d) P. L. Llewellyn, S. Bourrelly, C. Serre, A. Vimont, M. Daturi, L. Hamon, G. De Weireld, J. -S. Chang, D. -Y. Hong, Y. K. Hwang, S. H. Jhung and G. Férey, *Langmuir*., 2008, **24**, 7245-7250.

View Article Online
DOI: 10.1039/C8TA10610J

9 a) A. Sonnauer, F. Hoffmann, M. Fröba, L. Kienle, V. Duppel, M. Thommes, C. Serre, G. Férey and N. Stock, *Angew. Chem. Int. Ed*., 2009, **48**, 3791-3794; b) M. Lammert, S. Bernt, F. Vermoortele, D. E. De Vos and N. Stock, *Inorg. Chem*., 2013, **52**, 8521-8528; c) T. Wittmann, R. Siegel, N. Reimer, W. Millius, N. Stock and J. Senker, *Chem. Eur. J*., 2015, **21**, 314-323; d) A. E. Anderson, C. J. Baddeley and P. A. Wright, *Catal. Lett*., 2018, **148**, 154-163.

10 a) Y. Liu, J. F. Eubank, A. J. Cairns, J. Eckert, V. C. Kravtsov, R. Luebke and M. Eddaoudi, *Angew. Chem*., 2007, **119**, 3342-3347; b) M. Pang, A. J. Cairns, Y. Liu, Y. Belmabkhout, H. C. Zeng and M. Eddaoudi, *J. Am. Chem. Soc*., 2012, **134**, 13176-13179; c) M. Pang, A. J. Cairns, Y. Liu, Y. Belmabkhout, H. C. Zeng and M. Eddaoudi, *J. Am. Chem. Soc*., 2013, **135**, 10234-10237; d) D. Alezi, Y. Belmabkhout, M. Suyetin, P. M. Bhatt, L. J. Weselinski, V. Solovyeva, K. Adil, I. Spanopoulos, P. N. Trikalitis, A.-H. Emwas and M. Eddaoudi, *J. Am. Chem. Soc*., 2015, **137**, 13308-13318; e) Y. Belmabkhout, R. S. Pillai, D. Alezi, O. Shekhah, P. M. Bhatt, Z. Chen, K. Adil, S. Vaesen, G. De Weireld, M. Peng, M. Suetin, A. J. Cairns, V. Solovyeva, A. Shkurenko, O. El Tall, G. Maurin and M. Eddaoudi, *J. Mater. Chem A*., 2017, **5**, 3293-3303.

11 a) S. Yang, J. Sun, A. J. Ramirez-Cuesta, S. K. Callear, W. I. F. David, D. P. Anderson, R. Newby, A. J. Blake, J. E. Parker, C. C. Tang and M. Schröder, *Nat. Chem*., 2012, **4**, 887-894; b) T.-L. Hu, H. Wang, B. Li, R. Krishna, H. Wu, W. Zhou, Y. Zhao, Y. Han, X. Wang, W. Zhu, Z. Yao, S. Xiang and M. Schröder, *Nat. Commun*. 2012, **6**, 7328; c) S. Yang, A. J. Ramirez-Cuesta, R. Newby, V. Garcia-Sakai, P. Manuel, S. K. Callear, S. I. Campbell, C. C. tang and M. Schröder, *Nat. Chem*., 2015, **7**, 12-129; d) X. Han, H. G W. Godfrey, L. Briggs, A. J. Davies, Y. Cheng, L. L. Daeman, A. M. Sheveleva, F. Tuna, E. J. L. McInnes, J. Sun, C. Drathen, M. W. George, A. J. Ramirez-Cuesta. K. M. Thomas, S. Yang and M. Schröder*, Nat. Mater*., 2018, **17**, 691-696; e) C. P. Krap, R. Newby, A. Dhakshinamoorthy, H. García, I. Cebula, T. L. Easun, M. Savage, J. E. Eyley, S. Gao, A. J. Blake, W. Lewis, P. H. Beton, M. R. Warren, D. R. Allan, M. D. Frogley, C. C. Tang, G. Cinque, S. Yang and M. Schröder, *Inorg. Chem*., 2016, **55**, 1076-1088.

12 a) J. P. S. Mowat, S. R. Miller, A. M. Z. Slawin, V. R. Seymour, S. E. Ashbrook and P. A. Wright, *Microporous Mesoporous Mater*., 2011, **142**, 322-333; b) J. P. S. Mowat, V. R. Seymour, J. M. Griffin, S. P. Thompson, A. M. Z. Slawin, D. Fairen-Jimenez, T. Düren, S. E. Ashbrook and P. A. Wright, *Dalton Trans*., 2012, **41**, 3937-3941. c) A. J. Graham,

A. -M. Banu, T. Düren, A. Greenaway, S. C. McKellar, J. P. S. Mowat, K. Ward, P. A. Wright and S. A. Moggach, *J. Am. Chem. Soc.*, 2014, **136**, 8606-8613; d) L. Mitchell, B. G. -Santiago, J. P. S. Mowat, M. E. Gunn, P. Williamson, N. Acerbi, M. L. Clarke and P. A. Wright, *Catal. Sci. Technology*., 2013, **3**, 606-617; e) L. Mitchell, P. Williamson, B. Ehrlichová, A. E. Anderson, V. R Seymour, S. E. Ashbrook, N. Acerbi, L. M. Daniels, R. I. Walton, M. L. Clarke and P. A. Wright, *Chem. Eur. J*., 2014, **20**, 17185-17197; f) R. J. Marshall, C. T. Lennon, A. Tao, H. S. Senn, C. Wilson, D. Fairen-Jimenez and R. S. Forgan, *J. Mater. Chem. A*., 2018, **6**, 1181-1187.

13 I. A. Ibarra, X. Lin. S. Yang, A. J. Blake, G. S. Walker, S. A. Barnett, D. R. Allan, N. R. Champness, P. Hubberstey and M. Schröder, *Chem. Eur. J*., 2010, **16**, 13671-13679

14 a) S. R. Miller, P. A. Wright, C. Serre, T. Loiseau, J. Marrot and G. Férey, *Chem. Commun*., 2005, **0**, 3850-3852; b) J. P. S. Mowat, S. R. Miller, J. M. Griffin, V. R. Seymour, S. E. Ashbrook, S. P. Thompson, D. Fairen-Jimenez, A.-M. Banu, T. Düren and P. A. Wright*, Inorg. Chem*., 2011, **50**, 10844-10858; c) A. Greenaway, B. Gonzales-Santiago, P. M. Donaldson, M. D. Frogley, G. Cinque, J. Sotelo, S. A. Moggach, E. Shiko, S. Brandani, R. F. Howe and P. A. Wright, *Angew. Chem. Int. Ed*., 2014, **53**, 13483-13487; d) R. S. Pillai, V. Benoit, A. Orsi, P. L. Llewellyn, P. A. Wright and G. Maurin, *J. Phys. Chem. C*., 2015, **119**, 23592-23598 g) S. C. McKellar, J. Sotelo, A. Greenaway, J. P. S. Mowat, O. Kvam, C. A. Morrison, P. A. Wright and S. A. Moggach, *Chem. Mater*., 2016, **28**, 466-473; e) J. Sotelo, C. H. Woodall, D. R. Allan, E. Gregoryanz, R. T. Howie, K. V. Kamenev, M. R. Probert, P. A. Wright and S. A. Moggach, *Angew. Chem. Int. Ed*., 2015, **54**, 13332-13336.

15 a) J. Cepeda, S. Perez-Yáňez, G. Beobide, O. Castillo, E. Goikolea, F. Aguesse, L. Garrido, A. Luque and P. A. Wright, *Chem. Mater*., 2016, **28**, 2519-2528; b) J. Cepeda, S. Perez-Yáňez, G. Beobide, O. Castillo, A. Luque, P. A. Wright, S. Sneddon and S. E. Ashbrook, *Cryst. Growth. Des*., 2015, **15**, 2352-2363.

16 a) I. A. Ibarra, S. Yang, X. Lin, A. J. Blake, P. J. Rizkallah, H. Nowell, D. R. Allan, N. R. Champness, P. Hubberstey and M. Schröder, *Chem. Commun*., 2011, **47**, 8304-8306; b) X. Zhang, I. da Silva, H. G. W. Godfrey, S. K. Callear, S. A. Sapchenko, Y. Cheng, I. Vitorica-Yrezabal, M. D. Frogley, G. Cinque, C. C. Tang, C. Giacbbe, C. Dejoie, S. Rudic, A. J. Ramirez-Cuesta, M. A. Denecke, S. Yang and M. Schroder, *J. Am. Chem. Soc.* 2017, **139**, 16289-16296.

17 Y. Jiang, L. Sun, J. Du, Y. Liu, H. Shi, Z. Liang and J. Li, *Cryst. Growth. Des*., 2017, **17**, 2090-2096.

18 M. Krüger, R. Siegel, A. Dreischarf, H. Reinsch, J. Senker and N. Stock, *Microporous Mesoporous Mater*., 2015, **216**, 27-35.

19 *CrystalClear-SM Exper*t v2.1. Rigaku Americas, The Woodlands, Texas, USA, and Rigaku Corporation, Tokyo, Japan, 2015.

20 *CrysAlisPro* v1.171.39.8d. Rigaku Oxford Diffraction, Rigaku Corporation, Oxford, U.K. 2015.

21 Sheldrick, G. M. *Acta Crystallogr., Sect. A*. 2015, **71**, 3-8.

22 Sheldrick, G. M. *Acta Crystallogr., Sect. C*. 2015, ***71***, 3-8.

23 Spek, A. L. *Acta Crystallogr. Sect C*. 2015, **71**, 9-18.

24 Spek, A. L. *Acta Crystallogr. Sect D*. 2009, **65**, 148-155.

25 *CrystalStructure* v4.3.0. Rigaku Americas, The Woodlands, Texas, USA, and Rigaku Corporation, Tokyo, Japan, 2018.

26 V.A. Blatov, A.P. Shevchenko and D.M. Proserpio, *Growth Des.*, 2014, **14**, 3576–3586.

27 K. J. Pike, R. P. Malde, S. E. Ashbrook, J. McManus and S. Wimperis, *Solid State Nucl. Magn. Reson*., 2000, **16**, 203-215.

28 A. Gupta, S. Chempath, M.J. Sanborn, L.A. Clark and R.Q. Snurr, *Mol. Simul*., 2003, **29**, 29-46.

29 S.L. Mayo, B.D. Olafson and W.A. Goddard, *J. Phys. Chem*., 1990, **94**, 8897-8909.

30 A.K. Rappé, C.J. Casewit, K.S. Colwell, W.A. Goddard and W.M. Skiff, *J. Am. Chem. Soc*., 1992, **114**, 10024-10035.

31 http://chem-siepmann.oit.umn.edu/siepmann/trappe/index.html.

32 G. P. M. Bignami, Z. H. Davis, D. M. Dawson, S. A Morris, S. E. Russell, D. McKay, R. E. Parke, D. Luga, R. E. Morris and S. E. Ashbrook, *Chem. Sci*., 2018, **9**, 850-859.

33 K. Sumida, D. L. Rogow, J. A. Mason, T. M. McDonald, E. D. Bloch, Z. R. Herm, T. Bae and J. R. Long, *Chem. Rev*., 2012, **112**, 724-781.

34 A. Schoedel, M. Li, D. Li, M. O'Keeffe and O. M. Yaghi, *Chem. Rev*., 2016, **116**, 12466-12535.

View Article Online
DOI: 10.1039/C8TA10610J

35 a) J. Perles, M. Iglesias, C. Ruiz-Valero and N. Snejko, *Chem. Commun*., 2003, **0**, 346-347; b) A. Monge, F. Gándara, E. Gutiérrez-Puebla and N. Snejko, *CrystEngComm*., 2011, **13**, 5031.

36 Y. Qiu, H. Deng, S. Yang, J. Mou, C. Daiguebonne, N. Kerbellec, O. Guillou and S. R. Batten, *Inorg. Chem*., 2009, **48**, 3976-3981.

37 S.J. Ramsden, V. Robins and S.T. Hyde, *Acta Cryst. A* 2009, **65**, 81–108.

38 Y.-Q. Tian, Y.-M. Zhao, Z.-X. Chen, G.-N. Zhang, L.-H. Weng and D.-Y. Zhao, *Chem. Eur. J.* 2007, **13**, 4146-4154.

39 M. O'Keeffe, M. A. Peskov, S. J. Ramsden and O. M. Yaghi, *Acc. Chem. Res.* **2008**, *41*, 1782-1789.

40 V. R. Seymour, PhD Thesis, *University of St Andrews*, 2013.

41 R. Giovine, C. Volkringer, S. E. Ashbrook, J. Trébosc, D. McKay, T. Loiseau, J. -P. Amoureux, O. Lafon and F. Pourpoint, *Chem. Eur. J.*, 2017, **23**, 9525-9534.

42 H. Nebel, M. Neumann, C. Mayer and M. Epple, *Inorg. Chem*. 2008, **47**, 7874-7879.

43 The research data supporting this publication can be accessed at https://doi.org/10.17630/ce9f076e-083c-4226-a906-1cfb2abcafba.

View Article Online
DOI: 10.1039/C8TA10610J

TOC graphic and text

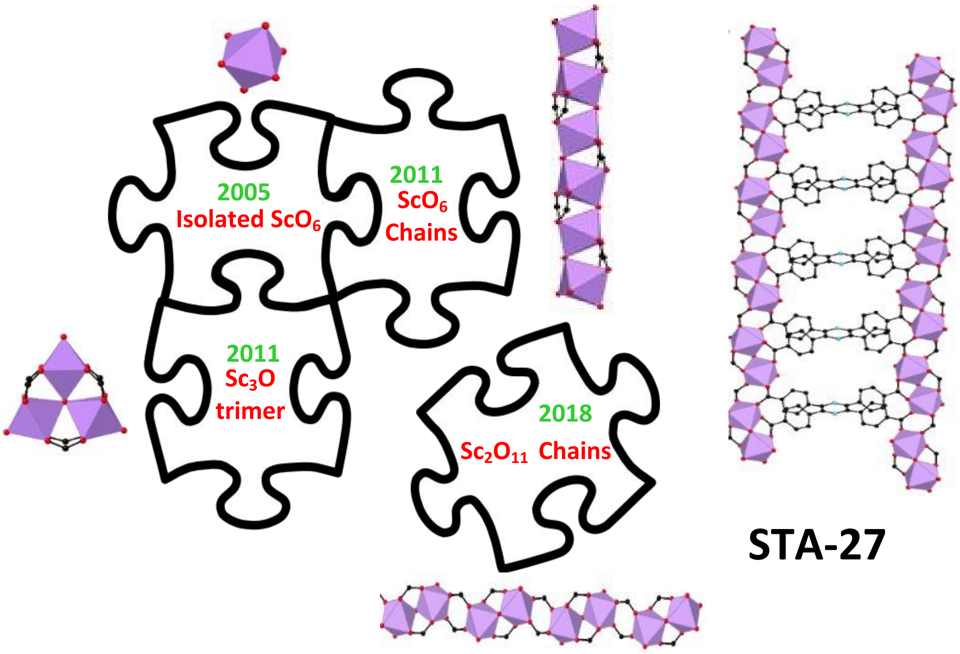

The scandium-based tetracarboxylate MOF STA-27, which contains a 1D rod SBU comprised of Sc_2O_{11} dimers, is an effective Lewis acid catalyst